TO APPEAR IN ASTROPHYSICAL JOURNAL
Preprint typeset using LaTeX style emulateapj v. 10/09/06

AEGIS: THE NATURE OF THE HOST GALAXIES OF LOW-IONIZATION OUTFLOWS AT $Z < 0.6$

TARO SATO[1,2], CRYSTAL L. MARTIN[2,3], KAI G. NOESKE[4], DAVID C. KOO[5], JENNIFER M. LOTZ[6]

(Received April 27, 2008; Accepted February 9, 2009)
Draft version April 20, 2009

ABSTRACT

We report on a signal-to-noise (S/N) limited search for low-ionization gas outflows in the spectra of the $0.11 < z < 0.54$ objects in the Extended Groth Strip (EGS) portion of the Deep Extragalactic Evolutionary Probe 2 (DEEP2) survey. Doppler shifts from the host galaxy redshifts are systematically searched for in the Na I λ 5890,96 doublet (Na I D). Although the spectral resolution and S/N limit us to study the interstellar gas kinematics from fitting a single doublet component to each observed Na I D profile, the typical outflow often seen in local luminous-infrared galaxies (LIRGs) should be detected at $\gtrsim 6\sigma$ in absorption equivalent width down to the survey limiting S/N (~ 5 pixel^{-1}) in the continuum around Na I D. The detection rate of LIRG-like outflow clearly shows an increasing trend with star-forming activity and infrared luminosity. However, by virtue of not selecting our sample on star formation, we also find a majority of outflows in galaxies on the red sequence in the rest-frame ($U-B$, M_B) color-magnitude diagram. Most of these red-sequence galaxies hosting outflows are of early-type morphology and show the sign of recent star formation in their UV-optical colors; some show enhanced Balmer Hβ absorption lines indicative of poststarburst as well as high dust extinction. These findings demonstrate that outflows outlive starbursts and suggest that galactic-scale outflows play a role in quenching star formation in the host galaxies on their way to the red sequence. The fate of relic winds, as well as the observational constraints on gaseous feedback models, may be studied in galaxies during their poststarburst phase. We also note the presence of inflow candidates in red, early-type galaxies, some with signs of active galactic nuclei/LINERs but little evidence for star formation.

Subject headings: galaxies: active — galaxies: evolution — galaxies: formation — galaxies: stellar content — ISM: jets and outflows

1. INTRODUCTION

A number of large-scale galaxy surveys of unprecedented volume and depth are steadily mapping out the luminous constituents of the universe out to higher redshifts. The lambda cold dark matter (ΛCDM) cosmological paradigm describes the gravity-driven assembly history of the universe quite successfully on the largest physical scales. Yet our understanding of the universe remains largely incomplete on the galaxy scales where the astrophysical processes involving stellar evolution and feedback of interstellar and intergalactic matter are essential — baryons can cycle through these in an intricate, multiphase manner. Gaseous feedback processes have been gaining serious attention, since theoretical predictions of the growth of luminous structure are highly sensitive to the "prescriptions" for these small-scale, subgrid physics (e.g., Croton et al. 2006; Bower et al. 2006; Hopkins et al. 2006), yet the observational constraints are still relatively scarce.

Absorption-line probes of the gas entrained in galactic "superwinds" (e.g., Chevalier & Clegg 1985; Heckman et al. 1990) have been effective in constraining how much matter could be carried by outflows through the lines in the rest-frame optical (e.g., Heckman et al. 2000; Rupke et al. 2002, 2005b; Martin 2005) and ultraviolet (e.g., Heckman et al. 2001; Schwartz et al. 2006), which may pollute intergalactic media and eventually deplete host galaxies of fuel for further star formation. The low-ionization absorption line studies suggest that a considerable amount of neutral gas may be carried away by outflows, $\sim 10^4$–10^7 $M_\odot$ in dwarfs (Schwartz & Martin 2004) and $\sim 10^8$–10^{10} $M_\odot$ in ultraluminous infrared galaxies (ULIRGs; Martin 2005; Rupke et al. 2005b). The column density of outflowing cool matter, however, can only be estimated after making a series of crude assumptions on its geometry, ionization state, dust-depletion factor, and metallicity. Although the reliability of such mass outflow estimates could therefore be questioned, an unambiguous detection of outflow is relatively straightforward in finding a Doppler-shifted absorption component in a line complex of interest. So far, a vast majority of existing studies of outflows have focused on galaxies selected a priori to have high star formation rates (SFRs), from dwarf starburst galaxies (e.g., Schwartz & Martin 2004) and luminous infrared galaxies (e.g., Martin 2005, 2006; Rupke et al. 2005a,b) in the local universe to Lyman-break galaxies at high redshifts (e.g., Shapley et al. 2003); see Veilleux et al. (2005) for a recent review. Although winds have been unambiguously detected in these systems, much work remains to be done in characterizing outflows in terms of their host galaxy properties in a large, relatively unbiased sample.

The Na I λ 5890,96 doublet (Na I D) absorption can be stellar or interstellar in origin yet is a useful line for a census of cool winds in the interstellar medium (ISM). Since it is an absorption line measured against the background light of host galaxies, its Doppler shift relative to the systemic redshift can be measured reasonably well. The Na I D absorption line directly traces cool ($T \sim 100$ K) gas which may directly fuel star formation. In (U)LIRGs, $\sim 10\%$ of the dynamical mass

[1] nomo17k@gmail.com
[2] Department of Physics, University of California, Santa Barbara, CA 93106-9530, U.S.A.
[3] Packard Fellow
[4] Keck Foundation Fellow; Harvard-Smithsonian Center for Astrophysics, Cambridge, MA, U.S.A.
[5] UCO/Lick Observatory, Department of Astronomy & Astrophysics, University of California, Santa Cruz, U.S.A.
[6] Leo Goldberg Fellow; National Optical Astronomical Observatories, Tucson, AZ, U.S.A

can be entrained in cool outflows (Rupke et al. 2005b; Martin 2006), suggesting that the bulk of outflowing mass resides at the cool phase. The Na I D doublet is a resonance line and forms among the most prominent absorption lines detectable out to $z \sim 0.5$ in optical spectra.

There is a pressing need to extend the study of outflows to the systems with lower SFRs as well as at later stages of star formation. For one thing, the observed spatial extent of outflows in local ULIRGs and a simple dynamical argument suggest that outflowing gas clouds may outlive starbursts or active galactic nuclei (AGNs) which may drive outflows (Martin 2006). Recently, Tremonti et al. (2007) found that $z \sim 0.5$ massive poststarburst galaxies, observed at up to 1.5 Gyr after intense episodes of star formation, host outflows almost as fast as or even faster than those observed in local ULIRGs. Since outflows may carry away from galaxies a significant fraction of gas mass that would otherwise be available for further star formation, knowing the "fate" of outflowing matter is clearly of interest.

In this paper, we present the result from a systematic search for Na I D outflows in a flux-limited sample of galaxies, drawn from the Extended Groth Strip (EGS) portion of the Deep Extragalactic Evolutionary Probe 2 survey (DEEP2; Davis et al. 2003). Since the EGS field has been extensively observed by a wide array of multiwavelength missions as part of the All-wavelength Extended Groth Strip Survey (AEGIS; Davis et al. 2007), we are able to characterize our spectroscopically selected sample in view of various physical quantities. Although Na I D is a resonance line and among the most prominent of absorption lines in the visible, rigorous absorption analysis needs high signal-to-noise (S/N) continuum, which is a requirement not quite satisfied by the vast majority of 1 hr integration spectra from the DEEP2 survey. Co-adding a number of low-S/N spectra from a set of subsamples to improve the effective S/N is a sensible approach. Yet even such stacking analyses are limited a priori by numerous ways in which subsamples can be constructed; some prior knowledge must be gained about the subsampling schemes in which the desired information can best be elucidated. In order to initiate an effort to carry out an unbiased census of outflows in modern spectroscopic galaxy surveys, as well as to motivate ensuing stacking analysis with proper subsampling schemes, it is still beneficial to take an approach to seek evidence of outflows in individual spectra.

An ambitious goal would be to estimate the quantities that are useful for improving the prescriptions of cosmological semianalytical simulations, such as outflow detection rate and mass-loading factor in a robust volume-limited sample. In this paper, however, our focus is on simply characterizing the property of galaxies that host LIRG-like outflows, using a rich set of multiwavelength observations from the AEGIS survey. We first describe the data, selection, and analysis method for the Na I D sample in § 2. The host galaxies of outflows, as defined from the Na I D kinematics, are then studied in view of their UV, optical, and infrared properties in § 3. We then note a few caveats, frame our findings in the larger context of galaxy evolution (§ 4), and summarize the paper (§ 5). Throughout this paper, we adopt the standard ΛCDM cosmology, $(\Omega_m, \Omega_\Lambda) = (0.3, 0.7)$, with $H_0 = 70$ km s^{-1} Mpc^{-1}.

2. DATA AND ANALYSIS

2.1. *DEEP2 Spectra*

The EGS, covering ≈ 0.5 deg^2, is one of the four fields observed in the DEEP2 survey (see Coil et al. 2004; Davis et al. 2003, 2004, for the descriptions of the survey), in which the spectroscopic targets are preselected by the Canada-France-Hawaii Telescope (CFHT) *BRI* photometry (Cuillandre et al. 2001). While the targets in the other three fields are preselected to the apparent magnitude limit of $R_{\rm AB} \leq 24.1$ and by color cuts to the galaxies likely to be at $z \gtrsim 0.7$, such a color cut was used in the EGS to slightly down-weight galaxies at $z \lesssim 0.7$, resulting by design in roughly equal numbers of galaxies above and below $z = 0.7$. The spectra for $\simeq 13,570$ EGS objects are obtained with the DEIMOS spectrograph on the Keck II telescope (Faber et al. 2003). The 1200 lines mm^{-1} grating centered at 7800 Å and the OG550 order-blocking filter with 1″ slit widths are used, which leads to the spectral coverage roughly of 6500–9100 Å. The spectral resolution in FWHM is ~ 68 km s^{-1}. The data are processed by an automated pipeline to produce (unfluxed) one-dimensional spectra (Newman et al., in preparation). The DEEP2 DEIMOS pipeline[7] produces an inverse-variance vector for each spectrum. In this paper, we use the spectra extracted via a variant of the optimal extraction algorithm presented in Horne (1986). Throughout this paper, we only use spectra which are tagged DEEP2 ZQUALITY flag of four.

2.2. *Systemic Redshifts*

An outflow velocity is measured relative to a systemic redshift of a host galaxy. A major contribution to the uncertainty of outflow velocity therefore comes from the uncertainty in the systemic redshift measurement. Each DEEP2 spectrum is assigned a spectroscopic redshift from χ^2 minimization with a few template spectra and has the accuracy well quantified from repeat observations (30 km s^{-1} in RMS; Willmer et al. 2006). Each redshift measurement has been visually inspected and assigned a redshift quality flag.[8] Nevertheless, we carry out independent redshift measurements using IRAF software package XCSAO (Kurtz & Mink 1998). The primary motivation for an independent set of redshift measurements is to mask the Na I D complex. The Na I D absorption line is among the most prominent features in the visible part of the galaxy spectrum. In the case where a systemic redshift should only reflect the centroid of the stellar motions, Na I D should be excluded from cross correlation with stellar spectral templates, in order to avoid the interstellar components, which may be redshifted or blueshifted from the systemic redshift of the galaxy, to affect the result.

We adapt the cross-correlation templates (ID: 24–30) from the fifth data release of the Sloan Digital Sky Survey (SDSS; Adelman-McCarthy et al. 2006). The template which yields the smallest uncertainty is generally picked and designated as the systemic redshift of the galaxy. An uncertainty in each redshift measurement is derived from the *r* statistics, which roughly corresponds to the S/N of cross-correlation peak from which the best redshift estimate is computed (Tonry & Davis 1979). The agreement between XCSAO and DEEP2 redshifts is generally good; for most purposes, the systematic redshift disparity of cz(XCSAO) − cz(DEEP2) ≈ 10 km s^{-1} is much less than the instrumental resolution and is insignificant. Where precise systemic redshifts are critical, we use XCSAO measurements, since the uncertainty is empirically calibrated and well understood among our sample. The redshift mea-

[7] http://astro.berkeley.edu/~cooper/deep/spec2d/
[8] See http://deep.berkeley.edu/ for the DEEP2 survey detail.

surement stored in each DEEP2 spectrum almost certainly underestimates the uncertainty in case of gross template mismatch, since only three components are used to generate a template for cross correlation, and χ^2 statistics was computed after continua are removed from them. Each redshift measurement for which $|cz(\mathrm{XCSAO}) - cz(\mathrm{DEEP2})| > 2\sigma_v(\mathrm{XCSAO})$ is visually inspected, and the spectrum is either reassigned a redshift from another template or removed from the sample. Only one object dropped out of the sample because of the failure in the cross-correlation redshift measurement.

2.2.1. *Spectral Line Indices*

Using the rest-frame band definitions in Table 1, we measure the spectral indices (denoted W_0, with the subscript "0" meaning rest frame) of some lines as estimates of their equivalent widths. Each spectral line index is computed via the "flux-summing" method. First, a straight line "pseudocontinuum" is fitted to the variance-weighted pixel flux values from the blue and red straddling continua as defined in Table 1, via the standard Levenberg-Marquardt algorithm. The covariance matrix is used to estimate the uncertainty in the pseudocontinuum. Then at each pixel i with a pixel width $\Delta\lambda_i$ in wavelength falling within the spectral bandpass defined as "line" in Table 1, the observed flux f_o and the pseudocontinuum flux f_c is used to compute the flux excess or depletion, such that

$$W = -\sum_i \left(\frac{f_o - f_c}{f_c}\right)_i \Delta\lambda_i$$

yields the equivalent width index in the observed frame. The rest-frame value is computed simply from $W_0 = W/(1+z)$ where z is the redshift of the galaxy. The uncertainty in the index is estimated by formal propagation of uncertainties in f_o and f_c using the above relation. By construction, $W_0 > 0$ Å (< 0 Å) corresponds to a line flux seen in absorption (emission), although the physical interpretation is slightly complicated by the fact that both emission and absorption may exist in a line feature, sometimes called emission filling. Although not perfect, a line index gives a good estimate of true equivalent width, when emission filling is not significant.

Previous studies have used the equivalent width of the Mg I b$\lambda 5167,73,85$ triplet to estimate the stellar contribution to the Na I D absorption line (Heckman et al. 2000; Rupke et al. 2002; Schwartz & Martin 2004; Rupke et al. 2005a; Martin 2005). The correlation between Na I D and Mg I b equivalent widths in stellar spectra is expected based on the similar mechanisms from which Na and Mg are produced in stars and their roughly similar ionization potentials (5.14 eV and 7.65 eV for Na and Mg, respectively). Heckman et al. (2000), Martin (2005), and Rupke et al. (2005a) all showed high equivalent width ratios of Na I D to Mg I b to be a good indicator of the presence of winds from their samples of infrared-luminous galaxies. This assumption is reasonable provided that a presence of a large column density from the interstellar Na I is required for a secure detection of outflow. In Fig. 1, however, we see evidence that a population of galaxies with outflows would be missed by a high W_0(Na I D)/W_0(Mg I b) selection scheme. The figure is meant to facilitate a comparison to the existing studies, in which the samples are selected by a high level of star formation (i.e., a high infrared luminosity). As will be discussed later, outflows appear to outlive starbursts, and the relic winds may present significant columns to be detected in poststarburst or post–star-forming galaxies.

TABLE 1
SPECTRAL LINE INDEX DEFINITIONS

Line	Blue continuum (Å)	Line (Å)	Red continuum (Å)
Hβ	4836–4846	4846–4878	4878–4888
Mg I b	5112–5142	5150–5200	5209–5239
Na I D	5822–5842	5881–5910	5910–5930

2.3. *Sample Selection*

We systematically search DEEP2 spectra in the EGS field for the coverage of Na I D absorption line and continuum around it (Table 1). An object is removed from our sample if the redshifted Na I D spectral range is at least partially outside the edge or falls on the gap between the blue and red CCD chips. This process reduces the sample to 2248 objects. The spectral baseline of DEEP2 observations restricts our sample to $0.11 < z < 0.54$.[9] For each DEEP2 spectrum, the continuum S/N per pixel [$(\mathrm{S/N})_{\mathrm{pix}}$] in the region around Na I D is defined to be the median $(\mathrm{S/N})_{\mathrm{pix}}$ computed from the pixel flux values and their inverse variances registered within the blue and red continua (Table 1). The main selection cut is made at $(\mathrm{S/N})_{\mathrm{pix}} > 5$ around Na I D, reducing the sample to 493 objects. We also remove the objects whose Na I D feature is severely compromised by sky emission or atmospheric absorption lines after visual inspection, reducing the sample to 431 objects. The latter cut tends to remove objects at specific redshifts where the redshifted Na I D overlaps with telluric features.

The particular choice of continuum S/N cut is a compromise between the inclusion of more objects for better statistics and the reliability of Na I D velocity measurements. Given the limited spectroscopic S/N, our desire to probe fainter objects is motivated by the well-known, downsizing nature of star formation (e.g., Cowie et al. 1996) and the apparent correlation between the presence of galactic-scale wind and the strength of star formation (e.g., Martin 2005; Rupke et al. 2005b). At low z, star formation is expected in optically fainter, low surface brightness galaxies. At high z, increasingly brighter galaxies are host to star formation yet become faint in their apparent brightness in the visible. We also expect that the high-S/N spectra are obtained from passive, early-type galaxies, which are generally of high surface brightness. All these effects conspire to make the galaxy population of interest to be somewhat elusive in the optical selection used here. Furthermore, the strength of Na I D absorption, both stellar and interstellar, varies widely from galaxy to galaxy, and our ability to detect an outflow depends on the strength of continuum as well as the absorption feature. It is therefore important to get some idea as to what kind of Na I D outflow to which our measurements are sensitive in this study.

In Fig. 2, the distribution of spectral index measurements as a function of continuum $(\mathrm{S/N})_{\mathrm{pix}}$ around Na I D is shown and demonstrates that we cannot obtain reliable Na I D velocity measurements in most spectra (i.e., constitutes the low-S/N sample; see § 2.4 for detail) at $(\mathrm{S/N})_{\mathrm{pix}} \lesssim 6.5$. The detection limit as a function of $(\mathrm{S/N})_{\mathrm{pix}}$ for a fiducial LIRG wind indicate that we are reaching the $\sim 6\sigma$ detection limit for a typical LIRG-type wind in our sample at that continuum S/N level. The distribution of low-S/N measurements suggests that we lose the ability to detect and measure the kinemat-

[9] Over the redshift range, the physical scale corresponding to 1″ slit varies from 2 kpc to 9.5 kpc.

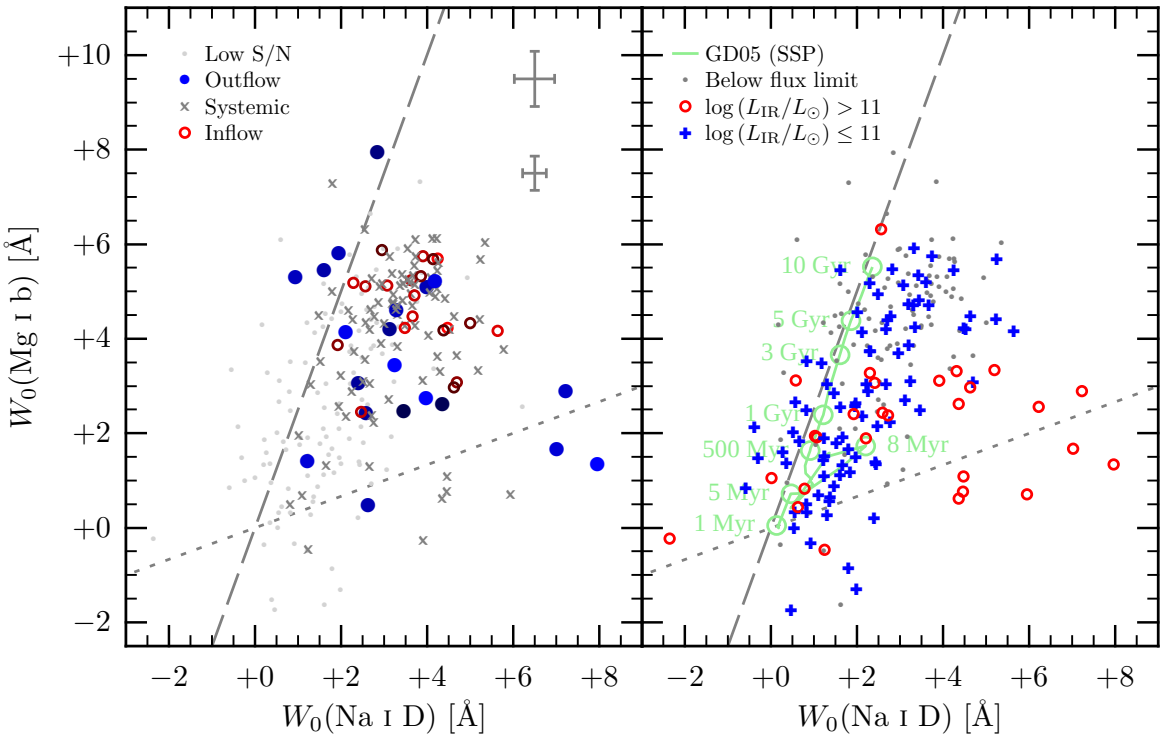

FIG. 1.— Mg I b-Na I D spectral index plane for the objects with the measurements of Na I D velocity (*left*) and the infrared luminosity (*right*). See § 2.2.1 for the definition of spectral indices. In the left panel, the points are denoted by Na I D kinematics into outflow (*blue filled circle*), systemic (*gray cross*), inflow (*red open circle*), and low S/N (*light gray dot*); see § 2.4.1 for the detail on Na I D kinematics. Outflows/inflow data points are color-mapped with the blueshift probability (§ 2.4.1), where bluer (redder) marks indicate stronger blueshift (redshift) of Na I D absorption line; see the inset of Fig. 3 for the exact color-mapping scheme with the blueshift probability. The error bars shown for the spectral indices are the medians for high- and low-S/N samples. In the right panel, the symbols indicate LIRGs (*red open circle*), non-LIRGs (*blue crosses*), and objects below flux limit of the *Spitzer*/MIPS 24 μm survey (*gray dot*). Rupke et al. (2005a) found most of their infrared-selected objects lying below the gray dotted line, W(Na I D) = 3W(Mg I b), to host outflows, whereas most objects above did not. The long gray dashed line indicates the fiducial stellar loci, W(Na I D) = 0.4W(Mg I b), where the slope was chosen to roughly match the evolutionary track of the solar-metallicity, single stellar population model from Delgado et al. (2005, *solid green line*). For each object the differences between the observed and fiducial stellar Na I D indices presumably indicate the interstellar contribution (see Fig. 5). (*A color version of this figure is available in the online journal.*)

ics of LIRG-like outflows at $(S/N)_{pix} \approx 5$. Thus the selection cut at $(S/N)_{pix} = 5$ seems justified, in terms of detecting LIRG-like winds at high ($\gtrsim 5\sigma$) confidence. Fig. 2 shows that the success rate of Na I D velocity measurement is a strong function of continuum $(S/N)_{pix}$. Overall, there are 205 objects with successful Na I D velocity measurements, and 226 objects without. We will describe what constitutes a "successful" (i.e., high S/N) velocity measurement in § 2.4.1.

2.4. *Modeling Na I D Absorption Lines*

In principle, countless possible configurations of the geometry of individual absorbers along a sightline give rise to an unlimited variety of observed Na I D absorption line profiles; from numerical simulations, several absorbers entrained in a starburst wind are expected to lie along a single sight line (A. Fujita et al. 2008, in preparation). In practice, however, the spectral resolution and moderate S/N limit our ability to study more than one component of Na I D doublet in the DEEP2 spectra; multiple absorption components would be seen blended even at a sufficient S/N. Due to the limitation, the physical quantities derived from a Na I D line profile in general may not be uniquely determined. Nonetheless, the modeling of the absorption line should be physically motivated, and in this respect we closely follow the method presented by Rupke et al. (2002, 2005a); readers are highly encouraged to find the detail of their absorption line analysis method in those papers. An absorption line is modeled with the wavelength (λ_c) and the optical depth (τ_0) at the line center, Doppler width (b_D), and the covering fraction (C_f) in a self-consistent manner. Our confidence intervals on Na I D velocity measurements, however, are obtained via directly carrying out the Markov chain Monte Carlo (MCMC) analysis on the observed spectra with the Rupke et al.-type line-profile modeling, rather than what Rupke et al. (2005a) outlines. In the Appendix, we give a summary of the technique, the analysis method, and the pipeline software developed for the task.

MCMC sampling generates a probability density for each model parameter which allows us to visually inspect the quality of our measurements. Except for a couple dozen high S/N spectra, the optical depths cannot be constrained at all, i.e., the probability density for the central optical depth τ_0 usually ends up being distributed roughly uniformly over the allowed range ($0 < \tau_0 < 999$) with a slight enhancement toward the lowest optical depths. In turn, the highly saturated profile tends to let the covering fraction C_f be distributed near the level of minimum intensity of a Na I D profile. This degeneracy between τ_0 and C_f at a low S/N regime is a well-understood property of the model profile employed by Rupke et al. and in this paper; extracting an optical depth in general requires a line shape to be very well sampled. The distributions of Na I D central wavelengths λ_c and Doppler widths b_D, on the other hand, are relatively well behaving even at lower S/Ns, where their probability densities roughly become Gaussian.

One especially important caveat of our Na I D velocity measurement is in order. Our interest is in studying the interstellar gas kinematics, so ideally stellar contributions to Na I D should be removed via such a method as fitting template

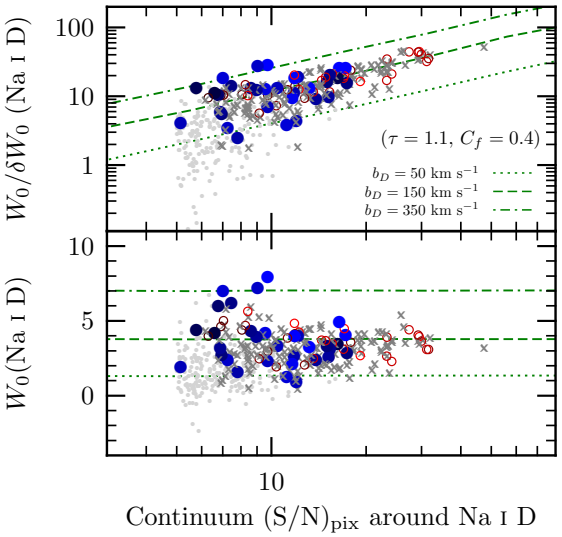

FIG. 2.— S/N (*top*) and spectral line index (*bottom*) as a function of continuum (S/N)$_{\rm pix}$ around Na I D. The points are denoted by Na I D kinematics: outflow (*blue filled circle*), systemic (*gray cross*), inflow (*red open circle*), and low S/N (*light gray dot*); see § 2.4.1 for the detail on Na I D kinematics. Outflows/inflow data points are color-mapped with the blueshift probability (§ 2.4.1), where bluer (redder) marks indicate stronger blueshift (redshift) of Na I D absorption line. The green lines are the loci of Na I D indices measured in the simulated DEEP2 spectra assuming fiducial Na I D absorption profiles expected from the fixed optical depth and covering fraction ($\tau = 1.1$ and $C_f = 0.4$) at three different Doppler widths [$b_D = 50$ (dotted green line), 150 (dashed green line), and 350 km s^{-1} (dash-dotted green line)], which are varied to simulate the effect of broadening in the absorption profile (*not* convolved with the instrumental resolution of ≈ 42 km s^{-1} here); see the Appendix for the definitions of the variables. The model with $b_D = 150$ km s^{-1} roughly reflects the mean Na I D property of LIRGs reported by Rupke et al. (2005b); i.e., the long dashed line in the upper panel indicates the significance of detection for a typical LIRG wind. For each model, a number of realizations are generated at a given S/N (i.e., a spectrum is degraded by Gaussian noise assuming that S/N) to obtain the uncertainty in the spectral index. (*A color version of this figure is available in the online journal.*)

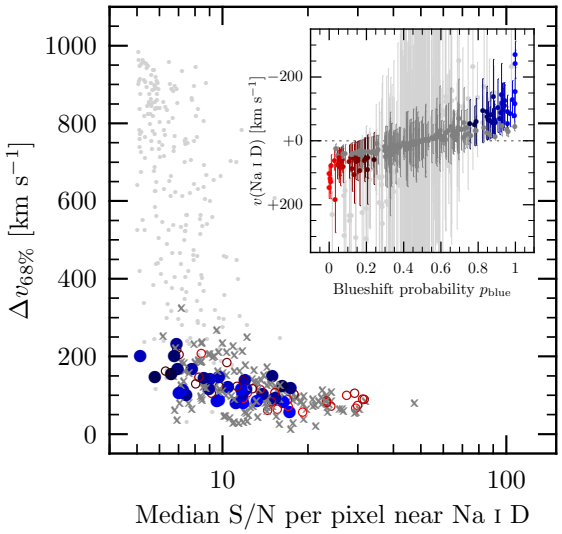

FIG. 3.— Distribution of Na I D velocity confidence intervals as a function of continuum (S/N)$_{\rm pix}$ around Na I D. Here $\Delta v_{68\%}$ is the difference of upper and lower 68% confidence limits in Na I D velocity. The symbols are as in Fig. 2. *Inset*: the Na I D velocity measurement with the error bar indicating the 68% confidence interval as a function of blueshift probability $p_{\rm blue}$. Outflows and inflows from the high-S/N sample are color-coded by blue and red, respectively, in gradient according to $p_{\rm blue}$ (sectNaID Velocity and Blueshift Probability); those at the systemic velocity are in gray. The low-S/N velocity sample (§ 2.4.1) are in light gray. High- and low-S/N velocity measurements are effectively separated in the ways that they are distributed in these plots, indicating the efficacy of the visual inspection scheme; see the text for detail. (*A color version of this figure is available in the online journal.*)

spectra generated from population synthesis models (e.g., Tremonti et al. 2004). The DEEP2 spectra are not rigorously fluxed, however, and we are unable to carry out a similar procedure. This is a substantial limitation in the analysis of galaxy spectra of intermediate- and old-age stellar populations, since their stellar absorption at Na I D becomes strong (Fig. 1; the stellar loci are from Delgado et al. (2005)). The implication on our definition of outflow velocity will be discussed in § 2.5.

We also do not take any special care of the nebular emission line He I λ 5876, found ~ 15 Å blueward of Na I D in some spectra. The He I emission line can contaminate the high-velocity tail of strong Na I D outflows in (U)LIRGs (e.g., Rupke et al. 2005a; Martin 2005). Upon visual inspection, however, few galaxies in our sample with a good Na I D velocity measurement are found to have their Na I D contaminated by the presence of the He I emission line.

2.4.1. *Na I D Velocity and Blueshift Probability*

Each Na I D central wavelength λ_c is converted to the Na I D velocity offset

$$v(\text{Na I D}) = c\frac{\lambda_c - \lambda_{\rm sys}}{\lambda_{\rm sys}}\ , \qquad (1)$$

where c is the speed of light and $\lambda_{\rm sys} = 5895.9243(1+z)$ Å is the line center of Na I D shifted to the observed frame using the cross-correlation redshift z. (The redder line of the doublet, Na I λ 5896, is used as the reference line throughout.) Using the above equation, the probability distribution of v(Na I D) is directly obtained from the probability distribution of λ_c from the MCMC sampling for each spectrum. In order to take into account the systemic redshift uncertainty, the probability distribution is further convolved by a Gaussian kernel having a width corresponding to the 1σ uncertainty in the cross-correlation redshift (in the velocity space) for each object. From each probability distribution, the best estimate for Na I D velocity is taken from the median, and the 68% confidence interval is likewise obtained.

For the purpose of measuring the Na I D velocity, the absorption feature detected at a sufficient S/N for such a measurement generally reveals itself as a normally distributed probability density in v(Na I D) well bounded within the parameter range, v(Na I D) = $\pm$700 km s^{-1}.[10] At a lower S/N, a probability distribution for v(Na I D) exhibits high- and low-velocity tails reaching the boundary values. Hence, after visual inspection, we divide our v(Na I D) measurements into two classes based on the behavior of v(Na I D) probability distribution: "high-S/N" velocity sample ($N = 205$) for which the distribution is well within $\pm$700 km s^{-1} and "low-S/N" velocity sample ($N = 226$) for which the distribution either extends to the boundary or is ill-behaving. Visual inspection also guards against the sampling results latching on to unwanted noise features, which usually show up as an abnormal probability distribution function. The MCMC measurement pipeline also allows a fitted absorption-line profile to be inspected for an interactively picked set of model parameters, so the integrity of the fitting result has also been visually checked

[10] While the Na I D outflow velocities outside this interval have been reported in literature (e.g., Rupke et al. 2005b; Martin 2005), the visual inspection of the velocity measurements indicates that the range of $\pm$700 km s^{-1} is sufficient for our sample, which does not include ULIRGs (with signs of AGN activities) in which the most very high velocity outflows are observed.

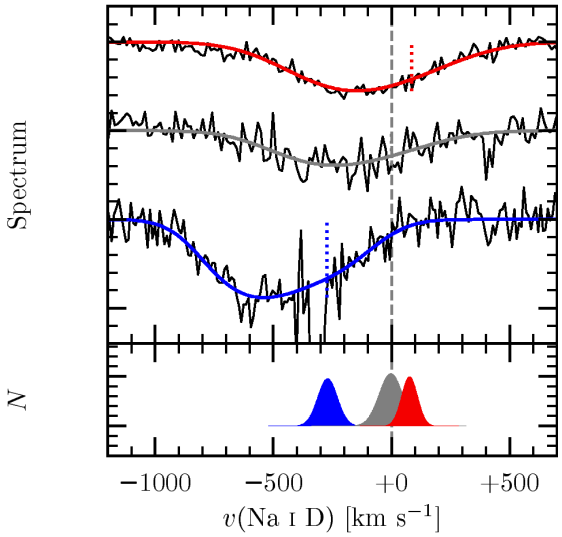

FIG. 4.— *Top*: examples of continuum-normalized spectra around Na I D (*black line*) and the best-fit models for the blueshift probability $p_{\rm blue} \simeq 1$ (*blue*), 0.5 (*gray*), and 0.01 (*red*). The vertical gray dashed line indicates the systemic velocity. The vertical dotted lines indicate the line center of Na I λ 5896 from the best-fit model for each spectrum. The 0 km s^{-1} corresponds to the systemic velocity of the red line of a blended doublet, and thus appears shifted toward red with respect to the centroid of a line profile even if the doublet itself is at systemic. *Bottom*: the probability distributions of Na I D velocity from the MCMC sampling; see § 2.4.1 for the detail on how the distributions are obtained. For the object showing a very strong outflow (*blue*), the probability distribution is entirely found at < 0 km s^{-1}, so the blueshift probability $p_{\rm blue}$ approaches unity. For a majority of galaxies, the distributions are roughly symmetric about 0 km s^{-1}, for which $p_{\rm blue}$ is about 0.5 (*black*). (*A color version of this figure is available in the online journal.*)

at various points in the distributions of model parameters; see the Appendix for detail. Fig. 3 shows the velocity width of confidence intervals ($\Delta v_{68\%}$; i.e., the difference between the upper and lower 68% confidence intervals) as a function of Na I D continuum $({\rm S/N})_{\rm pix}$. Since $\Delta v_{68\%}$ is a measure of the width of the probability distribution for v(Na I D), the figure shows that our strategy effectively distinguishes and separates out high- and low-S/N velocity measurements, which tend to appear at low and high $\Delta v_{68\%}$ regions, respectively.

Since we have robust probability density functions for v(Na I D), it is desirable to incorporate these into our definition of outflow detection, rather than relying heavily on the best estimates for v(Na I D). To do this, we introduce the *blueshift probability* $p_{\rm blue}$ for each velocity measurement, which is simply given by

$$p_{\rm blue} \equiv \int_{-\infty}^{0} dv \rho(v) \, ,$$

where $\rho(v)$ is the probability distribution function obtained from the MCMC sampling; recall that a blueshift yields a negative velocity in Eq. (1), so the distribution function needs to be integrated out to negative infinity to obtain the probability that a Na I D is seen blueshifted in a given spectrum. A few examples of observed Na I D absorption spectra, along with the probability distributions of Na I D velocity, are shown in Fig. 4 for the cases of $p_{\rm blue} \simeq 1$ (certainly an outflow), 0.5 (likely at systemic), and 0.01 (almost certainly "inflow"). The value of $p_{\rm blue}$ is a measure of how likely that a "real" Na I D velocity is blueshifted from the systemic velocity, given the result of MCMC sampling and the uncertainty in the systemic redshift of a host galaxy.

2.5. *Definition of Outflow*

To define what constitutes an outflow ("inflow") detection for the current analysis, we use a Na I D velocity cut of v(Na I D) < -50 km s^{-1} ($> +50$ km s^{-1}) and a blueshift probability cut of $p_{\rm blue} > 0.75$ (< 0.25). Readers are cautioned that, based on instrumental effects and data quality, precise definitions of outflows necessarily vary in the literature. The specific choice for the velocity cutoff is primarily motivated by the typical v(Na I D) uncertainty of ~ 50 km s^{-1} (Fig. 3) and the visual inspection of fitting results in relation to the values of v(Na I D) and $p_{\rm blue}$. Although a blueshift probability, by construction, should be an indicator of the likelihood of detecting an in/outflow at a desired confidence level, the additional velocity cutoff is used to guard against both the random and systematic errors in the redshift and the velocity measurements. For example, when the width of probability distribution function is narrow, i.e., $\Delta v_{68\%}$ is small, $p_{\rm blue}$ becomes more sensitive to the particular value of the systemic velocity. Upon visual inspection, we found that this often happened when a Na I D doublet line shape was less blended, and therefore the velocity moment could be determined more precisely. In such a case, an outflow as defined solely by a v(Na I D) distribution function looks dubious, having a tendency to be thrown off by an error in a *single* measurement of systemic redshift. Ideally, our systemic redshifts should also be scrutinized under rigorous MCMC analysis, which we did not carry out. For now, the additional velocity cut adequately achieves the same goal. The similar velocity cutoff was employed by Rupke et al. (2005b) to define outflow.

While employing a more stringent $p_{\rm blue}$ cut would yield a sample of outflows detected with higher confidence, we then seriously have to compromise our sample size. In order to take advantage of the large amount of data available in the AEGIS survey, our approach is to push the limit of detections down to an acceptably low confidence level. Hence our goal in this study is not to find individual cases of outflows or inflows *securely* but to give ourselves some statistical power to characterize the general properties of host galaxies. This is a compromise that we opt to consciously make.

As emphasized earlier, one caveat of the Na I D absorption analysis in this paper is our inability to remove the stellar contribution in the Na I D absorption (§ 2.4); a stellar fraction can only be estimated indirectly from such an index as Mg I b whose strength is known to correlate well with that of Na I D. Since the presence of interstellar absorber(s) is a necessary condition for outflows seen in absorption, some trend is expected to exist between the outflow detection rate and the interstellar fraction of the total Na I column. Fig. 5 shows that such a trend does exist, in which the objects with low Na I D stellar absorption fractions are more likely to host outflows (that we can detect). Without the explicit removal of stellar absorption components, however, the figure does not necessarily imply the paucity of outflows in galaxies whose Na I D is dominated by the stellar contribution. It is important to note again that our census is only sensitive to fairly strong outflows of the kind expected in LIRGs (Fig. 2). The kind of weak outflows observed by Schwartz & Martin (2004) in dwarf starbursts is certainly below the detection level of the present survey. Furthermore, since only one Na I D doublet component is fitted, the measured Na I D velocities are likely the lower limits to the kinematic component with the highest outflow velocity; each Na I D velocity is sensitive to the "moment" of multiple absorption components, at least one of which is stellar in origin and should exist at a systemic redshift. In high-S/N spectroscopy of (U)LIRGs, Rupke et al.

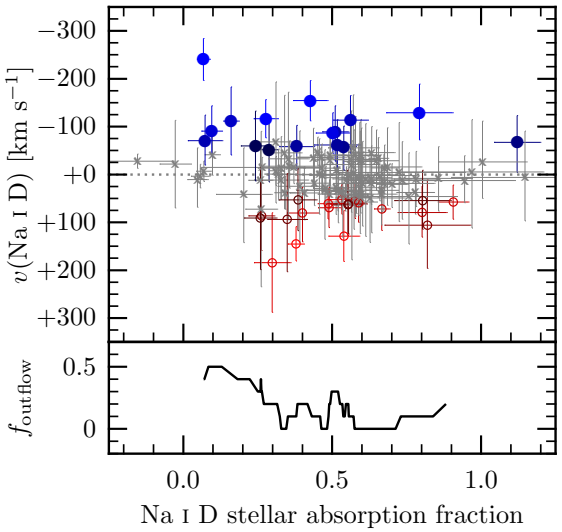

FIG. 5.— *Top*: Na I D velocity as a function of stellar fraction in the Na I D absorption index. The stellar fraction is given by W_*(Na I D)/W_0(Na I D), where the stellar absorption index is assumed to be W_*(Na I D) = 0.4W_*(Mg I b), so only the objects with both Na I D and Mg I b measurements are plotted; see the Mg I b-Na I D index plane (Fig. 1). For each object, the 1σ uncertainty in the stellar absorption fraction is estimated from resampling its locations on the Mg I b-Na I D index plane, drawn from a two-dimensional probability distribution to match the known W_0 uncertainties in Na I D and Mg I b. The objects for which the uncertainty in their stellar fraction is greater than 0.25 are not plotted. This removes three outflows that appear to the left of stellar loci in Fig. 1; either Na I D or Mg I b is contaminated by sky residuals in those objects, which cause their stellar fraction uncertainties to be very high (greater than 0.7). *Bottom*: the fraction of objects hosting outflows as a function of stellar fraction in the Na I D absorption index. The outflow fraction is computed at the sliding median of 10 adjacent objects. (*A color version of this figure is available in the online journal.*)

(2005a) and Martin (2005), for example, could fit more than one component of Na I D absorption in some spectra, provided that line profiles are not overly "smooth" due to blending and instrumental smearing. Fig. 5 indicates that our velocity measurements appear sensitive to outflows in Na I D when $\gtrsim$ 50% of the absorption equivalent width is interstellar in origin. Given these limitations, attaching a physical meaning to a Na I D velocity would be misleading, since it is only the *shift in the moment* of the absorption profile, not the isolated absorption from the outflowing/inflowing gas, to which our measurements are really sensitive. We thus avoid emphasis on the exact Na I D velocity values.

2.5.1. *Reality of "Inflows"*

The sensible cuts in the Na I D velocity and blueshift probability $p_{\rm blue}$ give rise to a population of galaxies with "inflows." While it would not be surprising to see an inflow from a sightline through an interacting system, "inflows" in our sample are seen mostly in luminous, massive galaxies in the red sequence (§ 3.2). The presence of inflows in these objects is striking. Given that these "inflow" detections are almost exclusively in early-type galaxies presumably with relatively little interstellar gas, we speculate whether factors other than interstellar absorption can cause potential systematics.

First, the precision of cross-correlation redshifts is generally worse with templates dominated by absorption lines, from which the redshifts of galaxies with "inflows" are obtained. It is also difficult to visually inspect redshift systematics in absorption-dominated spectra due to the lack of narrow, high-S/N features. As mentioned in § 2.2, a systematic velocity difference of order 10 km s^{-1} also exists between cross-correlation and DEEP2 redshifts, although this is small compared to inflow velocities. We do, however, take the redshift uncertainty into account in our definition of inflows (§ 2.4.1). Second, it might be possible that some unaccounted metal absorption features redward of Na I D may be causing systematics, redshifting the single-component Na I D profile fit. The experimentation with synthesis spectra from Bruzual & Charlot (2003) and Delgado et al. (2005) indicates that the degree of systematics would not be as strong as observed, assuming that Na I D and nearby metal lines are properly modeled. Third, as a significant fraction of galaxies with inflows appear to have lenticular morphology (Tremonti et al. 2007, private communication), another possibility is that a distinct kinematic component of *stellar* motion might be detected in these systems, perhaps from a faint disk.

While some of the above listed concerns are equally valid for outflows, in following sections we show compelling evidence that the detections of outflows are physically associated with star formation (or AGNs/LINERs). Such a clear physical connection cannot be made for inflows at present, and a preliminary investigation to explore the nature of the "inflow" population is underway. In radio ellipticals, neutral hydrogen is often seen in inflow, plausibly feeding the nuclear activity (e.g., van Gorkom et al. 1989); we do find some consistency with this scenario in our inflows. If these inflows are indeed associated with such feeding of AGNs, our method could provide an effective means of identifying the massive, early-type galaxies going through the "maintenance-mode" of AGN feedback. Nonetheless, we mostly defer the discussions of inflows to future papers.

2.6. *On Selection Effects*

Dependence on Na I D absorption strength. Our ability to measure a Na I D velocity depends primarily on the combination of the absorption and the continuum strengths, which introduces selection biases. Our main selection cut on continuum S/N around Na I D feature favors luminous, high surface brightness objects, which tend to be early-type galaxies on the red sequence (§ 3.2). Star-forming galaxies in the blue cloud are much fainter at $z \lesssim 0.5$ from which our sample is drawn. In Fig. 1, we see that high W_0(Na I D) objects tend to be old galaxies with a high stellar fraction or young galaxies with a high interstellar fraction in their Na I D absorption. Our survey lacks sensitivity to absorption lines in less luminous star-forming galaxies, where much of star formation occurs at $z \lesssim 0.5$. Therefore, that a significant fraction of our outflow detections is in red-sequence galaxies (§ 3.2) is partially a selection effect. Nonetheless, our sample nicely complements the existing studies of Na I D outflows which have focused on starburst galaxies.

Redshift dependence. Our sample consists of objects distributed over a fairly large redshift interval of $0.11 < z < 0.54$, and the analysis suffers from the problem typically encountered by a flux-limited survey. First, the observation becomes increasingly insensitive to fainter populations at higher redshift. Second, given a fixed opening angle, the survey volume tends to be smaller at lower z, and the sample variance (i.e., cosmic variance as galaxy enthusiasts like to say) becomes a serious issue; the survey field of view changes by a factor of ≈ 10 in physical area over the redshift interval. Third, the lookback time difference of several Gyr means that the galaxies experience a significant evolution over that redshift interval, so the lower- and higher-z populations characterized by one "fixed" physical property may not be of the same kind when looked at in view of other properties.

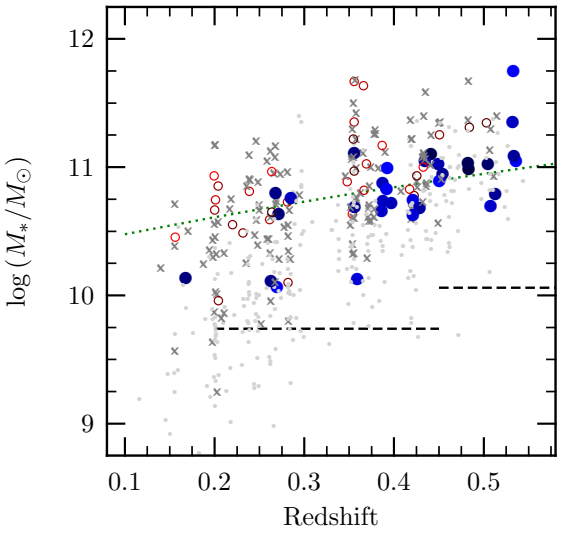

FIG. 6.— Stellar mass of galaxy as a function of redshift for the sample in this study. Each galaxy is coded by the Na I D kinematics (Fig. 3): outflow (*blue filled circle*), systemic (*gray cross*), inflow (*red open circle*), and low S/N (*light gray dot*). The horizontal dashed lines roughly indicate the 95% completeness limit in stellar mass computed at the centers of redshift intervals for $0.2 < z < 0.45$ and $0.45 < z < 0.7$ from Noeske et al. (2007a). The green dotted curve indicates the "quenching mass limit" as presented in Bundy et al. (2007). (*A color version of this figure is available in the online journal.*)

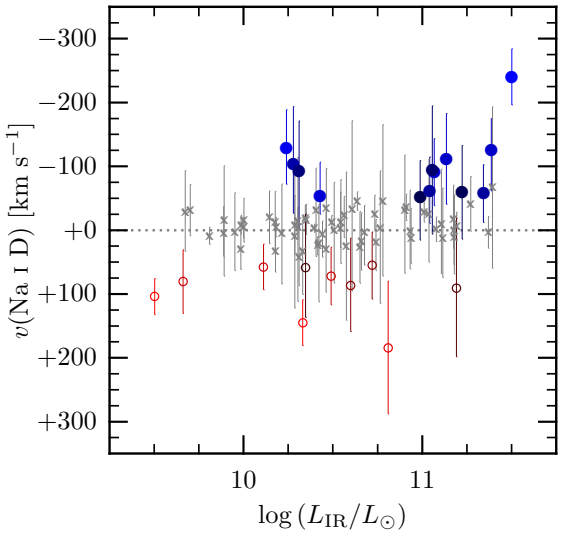

FIG. 7.— Na I D velocity as a function of infrared luminosity for the objects in the high-S/N sample (§ 2.4.1). The figure includes only the objects that are covered by the *Spitzer*/MIPS observations and are detected above the flux limit ($S_{24} \sim 83\mu$ Jy) to yield the measurements of $L_{\rm IR}$. The symbols are as in Fig. 2. (*A color version of this figure is available in the online journal.*)

TABLE 2
DETECTION RATES FOR NA I D OUTFLOWS SELECTED BY $L_{\rm IR}$

Criterion	$N_{\rm subsample}$	$N_{\rm outflow}$	Detection Rate
Within MIPS coverage	169	24	0.14 ± 0.03
$\log(L_{\rm IR}/L_\odot) > 11$	21	8	0.38 ± 0.11
$\log(L_{\rm IR}/L_\odot) \leq 11$	64	5	0.08 ± 0.03
No 24μ detection	84	11	0.13 ± 0.04

NOTE. — The conventional cut for LIRGs is $\log(L_{\rm IR}/L_\odot) > 11$. Only the objects with high-S/N Na I D velocities are included for the calculation of detection rates; i.e., the objects in the low-S/N sample (§ 2.4.1) are treated as if they are not detected. The uncertainties are estimated from binomial statistics.

Some insights into these effects are gained from Fig. 6. Apparently, the high-S/N sample (§ 2.4.1) does not come close to the completeness limit in stellar mass of the parent AEGIS survey, except at the lowest redshifts. The lower sampling rate of high-mass galaxies (e.g., $\log(M_*/M_\odot) \gtrsim 11$) at low redshift may be a result of the smaller survey volume; that is, luminous early-type galaxies tend to be highly clustered (e.g., Coil et al. 2008), and a smaller number of overdense regions with bright ellipticals fall in the field of view toward lower redshift. The effect of the changing physical aperture size, from 2 kpc to 9.5 kpc corresponding to the $1''$ slit, on the detectability of outflow is difficult to assess. The work by Martin (2006) on the spatially resolved Na I D outflows in local ULIRGs indicates that the extended blueshifted interstellar absorption is found over the scale of $\gtrsim 15$ kpc, in which case a significant column should remain available within the regions covered by the slit over the redshift range covered in this study.

3. HOST GALAXIES OF OUTFLOWS

3.1. *Trends with Star Formation*

Since the recent advance in the detailed knowledge of starburst-driven galactic winds have been gained through the studies of local LIRGs (e.g., Heckman et al. 2000; Rupke et al. 2002, 2005a,b; Martin 2005), the Na I D velocity measurements as a function of infrared luminosities $L_{\rm IR}$ naturally provide a starting point for comparison. Since for star-forming galaxies the infrared is dominated by the thermal dust emission of reprocessed starlight from hot, young massive stars, a tight correlation exists between $L_{\rm IR}$ and SFR in dusty star-forming galaxies (Kennicutt 1998). For a subset of our sample, the far-infrared photometry from *Spitzer*/Multiband Imaging Photometer (MIPS; Rieke et al. 2004) is used to derive the total infrared luminosity $L_{\rm IR}$, following Le Floc'h et al. (2005) and using the Chary & Elbaz (2001) spectral energy distribution (SED) templates.

In Fig. 7, a clear tendency is observed for high $L_{\rm IR}$ objects to host outflows. Indeed, a majority of outflows are found in LIRGs ($L_{\rm IR} > 10^{11}\ L_\odot$) in the figure. Table 2 presents the outflow detection rates for the subsampling based on $L_{\rm IR}$. The outflow detection rate of $38\% \pm 11\%$ for LIRGs is similar to those reported by low-z surveys of infrared-selected galaxies; e.g., $42\% \pm 8\%$ in Rupke et al. (2005b) and $32\% \pm 12\%$ in Heckman et al. (2000). Hence we confirm the results reported by others that the detection rate of outflow in infrared-selected galaxies correlates well with their infrared luminosity. We note, however, that the exact values for the detection rates, especially among the galaxies with lower $L_{\rm IR}$, may not be robust against selection effects and incompleteness, since our primary selection cut is made by the strength of continuum around Na I D (§ 2.3). There are no ULIRGs [$\log(L_{\rm IR}/L_\odot) > 12$] in our sample, which is reasonable given the expected number of ULIRGs in the survey volume is very small ($\lesssim 10$), assuming redshift-dependent luminosity functions of infrared sources (Le Floc'h et al. 2005) and the completeness of the DEEP2 survey.

In Fig. 8, the Na I D velocity as a function of the total SFR (i.e., the sum of SFRs derived from infrared SED and optical emission lines; see Noeske et al. (2007a) for details) is shown. The similar dependence of v(Na I D) on $L_{\rm IR}$ and the total SFR is expected due to the tight correlation between $L_{\rm IR}$ and the total SFR, which is often dominated by the infrared contribution. Again, a majority of outflows are seen in galaxies with SFR $\gtrsim 20\ M_\odot\ {\rm yr}^{-1}$, which correspond to the amount of SFR expected in LIRGs. As a caveat, it should be mentioned

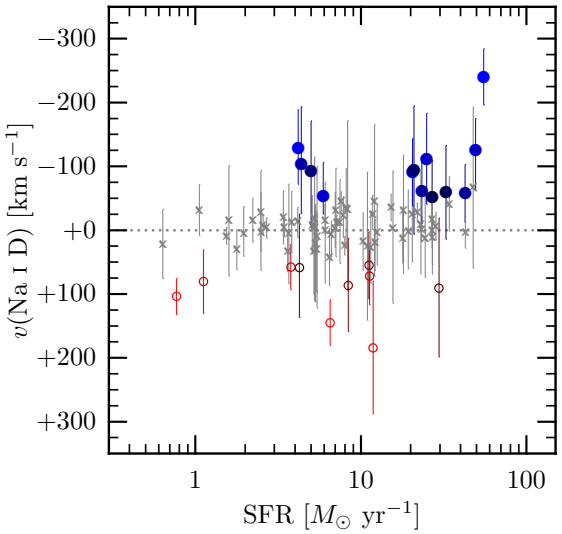

FIG. 8.— Na I D velocity as a function of total SFR, i.e., the sum of SFRs from the infrared emission and optical emission lines (§ 3.1). The symbols are as in Fig. 2. The SFR corresponding to that of LIRG ($L_{\rm IR} > 10^{11}\ L_\odot$) is $\approx 17\ \dot{M}_\odot$ yr^{-1}; see Fig. 7 for comparison. (*A color version of this figure is available in the online journal.*)

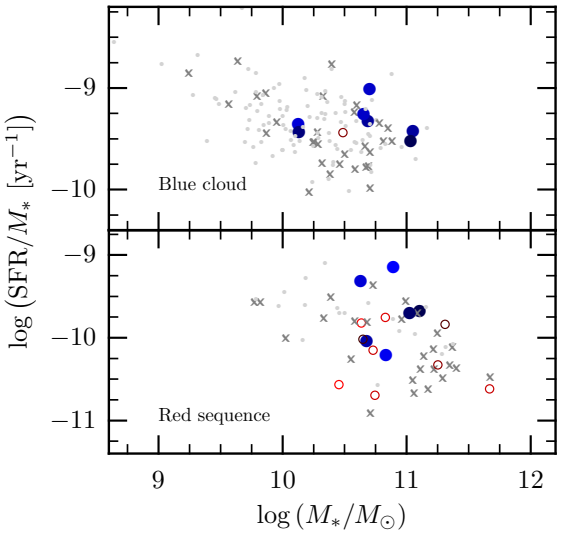

FIG. 9.— Specific SFR as a function of stellar mass for blue-cloud (*top*) and red-sequence (*bottom*) galaxies; see § 3.2 for the color cut scheme. The symbols are as in Fig. 2. The figure is comparable to Fig. 1 of Noeske et al. (2007b), except that red AGN/LINER candidates are not removed. An SFR estimate from optical line emission suffers significantly from AGN/LINER contamination (Yan et al. 2006; Weiner et al. 2007); therefore, their specific SFRs are likely overestimates here, especially for the red-sequence galaxies. (*A color version of this figure is available in the online journal.*)

that some of the infrared luminosity might be from (obscured) infrared-bright AGN, and not from star formation. We lack the diagnostics to distinguish star formation from AGN, but the simple relation between $L_{\rm IR}$ and SFR may not hold for the cases in which AGN contributions to the infrared luminosities are high. Local studies of LIRGs suggest that strong AGN contamination may be small, though low-luminosity AGN could be common (e.g., Veilleux et al. 1995).

Since the SFR scales almost proportionally with galaxy mass (e.g., Brinchmann et al. 2004), its inference with respect to the specific amount of star-forming activity may be misleading. The birthrate parameter, $b \equiv {\rm SFR}/\langle {\rm SFR} \rangle$ (Kennicutt 1998), is a better indicator which takes into account the star formation history yet is difficult to estimate due to its dependence on the timescale over which the galaxy has been forming stars as well as on the fraction of gas recycled in the past. It is still desirable to remove the first-order effect of galaxy mass, since our sample is drawn over the redshift interval where downsizing affects star formation particularly strongly. Specific SFR, defined as SFR$/M_*$ (i.e., SFR per unit stellar mass) is easier to compute and a reasonable proxy for birthrate parameter. Fig. 9 shows how the specific SFRs are distributed as a function of galaxy stellar mass M_*, obtained from fitting SEDs to optical and near-infrared photometry (Bundy et al. 2006). For the red-sequence galaxies (Fig. 10), the specific SFRs may be overestimated due to AGN/LINER contamination (Yan et al. 2006; Weiner et al. 2007). Focusing on the blue-cloud galaxies, an interesting feature is that, at a fixed mass, a majority of the objects with outflows are seen at the upper envelope of the distribution of specific SFRs. The analysis of the parent AEGIS sample by Noeske et al. (2007a,b) indicates that, in the redshift interval $0.11 \lesssim z \lesssim 0.55$ from which our sample is drawn, $M_* \sim 10^{11}\ M_\odot$ is roughly where star formation is seen to be quenched in the most massive galaxies. In the full Noeske et al. (2007b) sample, the distribution of star-forming galaxies is fairly tight; the loci in Fig. 9 suggest that host galaxies of outflows are undergoing an enhanced episode of star formation, relative to the star-forming galaxies without outflows at the same epoch.

It is emphasized that star formation may not be the only source of optical/infrared emission in the presence of an AGN. We see that quite a few red-sequence galaxies with *inflows* show up in the figures involving SFRs presented in this section. As discussed in the next section, these objects show little evidence of ongoing star formation in UV diagnostics, and most are either quiescent or show Seyfert/LINER-like excitation in their [N II]/Hα emission line ratios (§ 4.3). Hence inflows in general are more likely to be associated with AGN/LINERs than star formation.

3.2. *Color Magnitude Diagram*

Although optical photometry only tells an incomplete history, dividing galaxies into blue and red populations by optical colors still is very useful for capturing the essence of galaxy evolution with a bird's-eye view, since the bimodality of galaxy color distribution is among the most prominent features that persist over wide ranges of parameters, such as galaxy mass, luminosity, environment, and redshift (e.g., Baldry et al. 2004; Balogh et al. 2004; Willmer et al. 2006; Cooper et al. 2007). Over the past few decades, numerous studies of local galaxies have shown that the "red sequence" is generally populated by red, dead, passively evolving galaxies with old stellar populations, while the "blue cloud" is populated by blue, actively star-forming galaxies. These two densely populated regions are divided by a sparsely populated area, sometimes called the "green valley"; see Faber et al. (2007) and references therein for a comprehensive account.

Fig. 10 presents the rest-frame $(U-B, M_B)$ color-magnitude diagram, in which the host galaxies of outflows are seen in relation to the red sequence and the blue cloud. The catalog of rest-frame photometry was constructed as described in Willmer et al. (2006).[11] Given that the low-z red sequence galaxies are characterized as inactive and quiescent, that a majority of outflows are found in red galaxies comes as a surprise; among 32 outflows, 21 of them are found on the red

[11] The optical photometry are on the Vega system. See Willmer et al. (2006) for the conversion procedure between Vega and AB magnitudes.

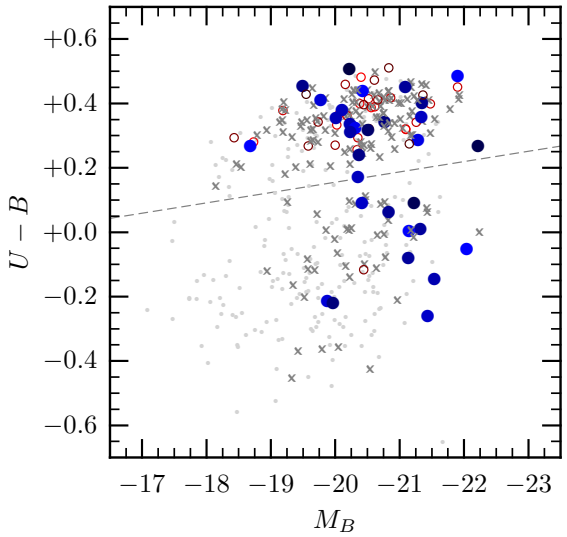

FIG. 10.— Rest-frame ($U-B$)-M_B color-magnitude diagram. The photometry, on the Vega system, is corrected for Galactic extinction but not for the internal extinction of galaxies; see Willmer et al. (2006) for detail. The symbols are as in Fig. 2. The dashed line indicates the $U-B$ color cut used to divide red-sequence and blue-cloud galaxies; see Faber et al. (2007). [*See the electronic edition of the paper for a color version of this figure.*]

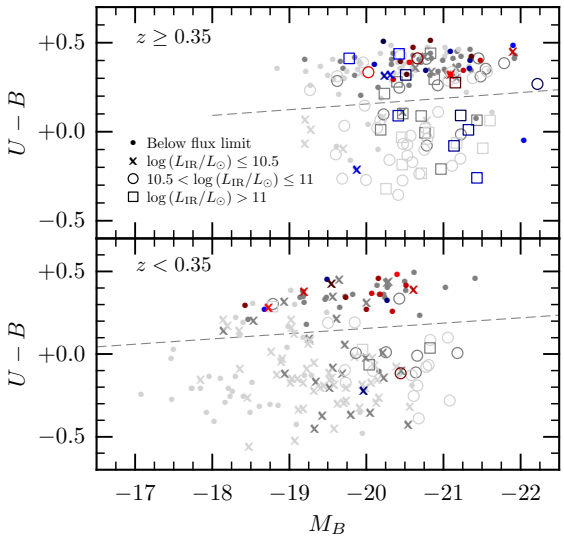

FIG. 11.— Rest-frame ($U-B$)-M_B color-magnitude diagram for objects at $z \geq 0.35$ (*top*) and $z < 0.35$ (*bottom*). The gray dashed lines divide red and blue galaxies (Fig. 10). The symbol indicates the infrared luminosity $L_{\rm IR}$: below flux limit (*dot*), $\log(L_{\rm IR}/L_\odot) \leq 10.5$ (*cross*), $10.5 < \log(L_{\rm IR}/L_\odot) \leq 11$ (*open circle*), and $\log(L_{\rm IR}/L_\odot) > 11$ (*open square*). The color scheme for the symbols is similar to Fig. 2 and indicates Na I D kinematics: outflow (*blue*), inflow (*red*), systemic (*gray*), and low S/N (*light gray*). There are roughly equal number of objects above and below the redshift cut at $z = 0.35$. [*See the electronic edition of the paper for a color version of this figure.*]

sequence. Non–star-forming, quiescent galaxies are red in the rest-frame optical due to their intrinsic SEDs; the rest-frame $U-B$ in particular brackets the 4000 Å feature, which is sensitive to the "break" caused by the Balmer limit, as well as the high metal opacity in the cool stellar atmosphere of old stars. Nonetheless, high dust reddening can push some star-forming galaxies into the red sequence, especially at higher redshift (e.g., Weiner et al. 2005; Bell et al. 2005). The rest-frame photometry in Fig. 10 are not corrected for the internal extinction of galaxies, so the "contamination" from dust-reddened star-forming galaxies can happen though expected to be small at $z < 0.5$. We also reiterate that, due to the fixed continuum S/N cut, our sample is naturally biased for red-sequence galaxies, which tend to have high surface brightness (§ 2.3). This selection bias due to the continuum strength can be inferred from the difference in the outflow detection rates for red and blue subpopulations. Among the full sample ($N = 431$), the outflow detection rates are $11/205 = 0.05 \pm 0.02$ and $21/226 = 0.09 \pm 0.02$ for blue and red objects, while they are $11/51 = 0.22 \pm 0.06$ and $21/154 = 0.14 \pm 0.03$ among the high-S/N sample ($N = 205$).

Fig. 11 shows the color-magnitude diagram in which the objects are denoted by their infrared luminosity and offers evidence that star-forming galaxies do reside in the red sequence, though relatively small in fraction. The sample is divided at $z = 0.35$ into low- and high-redshift subsamples, which makes clear that the infrared-luminous galaxy fraction is much greater at higher redshift, consistent with lookback-time studies of star-forming, infrared-luminous galaxies (e.g., Bell et al. 2005; Le Floc'h et al. 2005; Noeske et al. 2007a). Outflows are mostly observed in $z > 0.35$ objects. A comparison of the top and bottom panels shows quite strikingly that the $z > 0.35$ red sequence has a substantial number of infrared-luminous galaxies, some of which are LIRGs, which is absent in the $z < 0.35$ red sequence. The red-sequence outflows, however, are also found in the objects without significant 24 μm flux.

While the narrow spectral baseline of DEEP2 makes the Balmer decrement unavailable, the UV spectral slopes β from

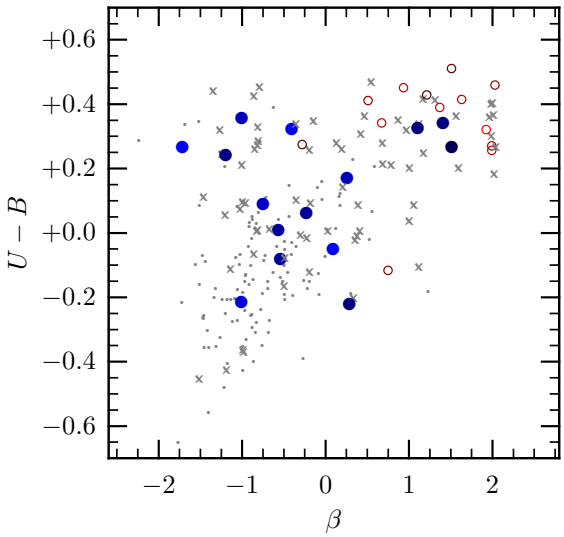

FIG. 12.— Rest-frame $U-B$ color as a function of the UV spectral slope β for a subset of objects with GALEX photometry. The β follows the definition given by Seibert et al. (2005), $f_\lambda \propto \lambda^\beta$; star-forming galaxies have smaller values of β due to their rising continua toward shorter wavelengths. The symbols are as in Fig. 2. A majority of blue-sequence galaxies are classified as low-S/N; they are bright in UV but fainter in the visible, making it difficult to obtain their high-S/N spectra. (*A color version of this figure is available in the online journal.*)

the *Galaxy Evolution Explorer* (GALEX) photometry are measured for a subset of our sample.[12] The UV spectral slope is generally a good measure of dust reddening, since it is a direct measure of continuum slope in ultraviolet, where dust optical depth is particularly high. Fig. 12 shows that some red galaxies with outflows have $\beta \lesssim 0$, comparable to typical blue star-forming galaxies. None of these with 24 μm detection, however, are LIRGs. Another look into their iden-

[12] The images were processed using ver. 4.1 of *GALEX* pipeline; see http://www.galex.caltech.edu.

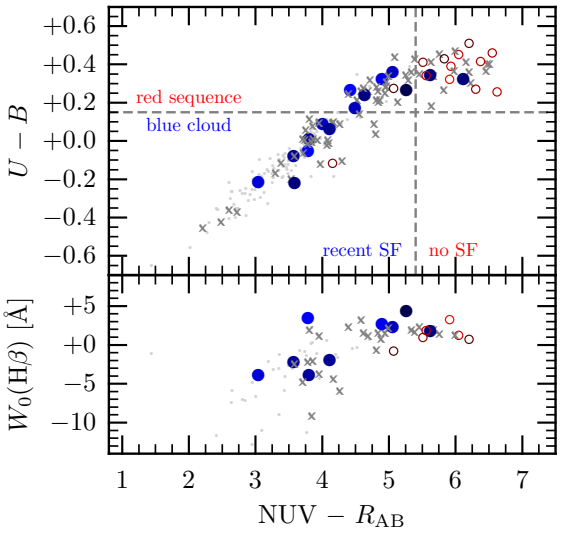

FIG. 13.— *Top*: rest-frame $U-B$ color as a function of rest-frame NUV$-R_{\rm AB}$ color. The horizontal dashed line at $U-B$ = 0.15 roughly divides red-sequence and blue-cloud galaxies (Fig. 10). The vertical dashed line at NUV$-R_{\rm AB}$ = 5.4 follows the delineation of star-forming and non–star-forming galaxies employed by Schawinski et al. (2006), who used NUV$-r$; r is roughly comparable to $R_{\rm AB}$. The symbols are as in Fig. 2. *Bottom*: Hβ spectral line index as a function of rest-frame NUV$-R_{\rm AB}$ color for a subset of objects with the Hβ coverage. The strength of Hβ absorption [i.e., $W_0(\mathrm{H}\beta) \gtrsim 0$ Å] is sensitive to a starburst occurred within $\sim 10^7$ Myr–2 Gyr ago (see the inset of Fig. 14). A negative $W_0(\mathrm{H}\beta)$ indicates the presence of emission at Hβ, i.e., W_0 is an estimate of the sum of emission and absorption equivalent widths (§ 2.2.1). (*A color version of this figure is available in the online journal.*)

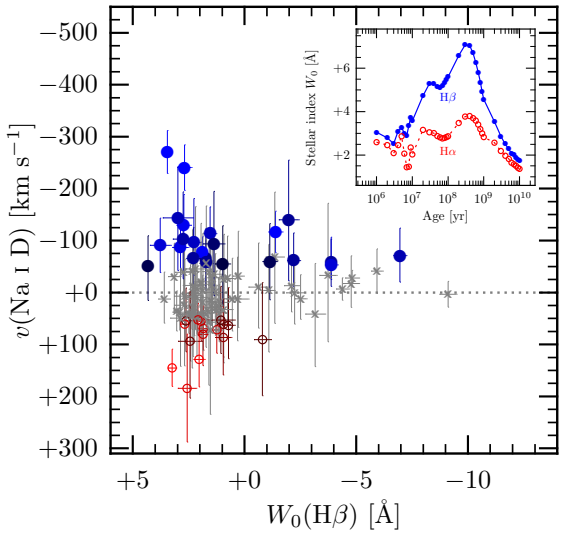

FIG. 14.— Na I D velocity as a function of Hβ spectral line index. The symbols are as in Fig. 2. Since the Hβ index measures the sum of absorption and emission lines, the Hβ index becomes a lower limit to the strength of Hβ absorption equivalent width, if emission filling is significant. In turn, $W_0(\mathrm{H}\beta) \lesssim 0$ Å indicates that the emission line flux is greater than that of absorption line. See § 2.2.1 for detail on the definition of the spectral line index. *Inset*: the stellar spectral line index at Hα (*red dashed line*) and Hβ (*blue solid line*) as a function of stellar ages. The indices are measured from a single stellar population model from Delgado et al. (2005). A stellar population with the age $\gtrsim 10$ Gyr has $W_0(\mathrm{H}\beta) \approx 2$ Å. An Hβ index $\gtrsim 3$ Å is expected for a stellar population during a poststarburst phase from ~ 10 Myr up to ~ 2 Gyr. (*A color version of this figure is available in the online journal.*)

tity is given by the top panel of Fig. 13, where the distribution of galaxies in their rest-frame $U-B$ color is compared to that of the rest-frame NUV$-R_{\rm AB}$ color. The UV-optical color is much more sensitive to a small fraction of young stellar populations and in turn the current as well as recent star-forming activity than optical colors alone. The particular NUV$-R_{\rm AB}$ cut delineating star formation from no star formation is from Schawinski et al. (2006), who used NUV$-r$ colors; SDSS r is close to CFHT $R_{\rm AB}$. In this empirical color cut, early-type galaxies with the strongest UV upturn observed locally should not contaminate the star-forming classification; this makes inevitable that some objects in the "no star formation" region may actually be star forming. Based on the cut, Schawinski et al. found that $\sim$ 30% of visually classified $z < 0.1$ early-type galaxies brighter than $M_r = -21.5$ showed signs of recent star formation. Strikingly, most optically red galaxies with outflows have NUV$-R_{\rm AB} < 5.4$, suggestive of recent star formation.

These results give rise to an interpretation that the arrival on the red sequence of the galaxies with outflows happened only recently; i.e., red sequence outflows are found predominantly in post–star-forming galaxies with detectable residual star formation or dusty star-forming galaxies with high infrared emission. The redness in their visible colors might also arise partly from the presence of dust; the strong correlation between reddening $E(B-V)$ and the equivalent width of low-ionization absorption lines are often reported (e.g., Armus et al. 1989; Veilleux et al. 1995; Heckman et al. 2000). Poststarburst galaxies, identified spectroscopically by their strong Balmer absorption, are generally found to be dusty as well (e.g., Poggianti & Wu 2000; Poggianti et al. 2001; Balogh et al. 2005; Sato & Martin 2006). The appearance of the post–star-forming phase also fits well with the scenario that it is observed when star-forming galaxies in the blue cloud make the transition to the red-sequence after some mechanism triggered an enhanced episode of star formation, which then gets shut off. The NUV$-R_{\rm AB}$ color alone, however, does not rule out low-level star formation in these galaxies, since whether a galaxy goes through poststarburst depends on the fraction of mass that has formed in the most recent star formation event as well as its timescale. It is also worth noting the clear separation between outflows and inflows in NUV$-R_{\rm AB}$; most inflows are observed in red galaxies in which little or no star formation is detected.

3.3. *Evidence for Poststarburst*

The Balmer absorption lines are sensitive to the age of the underlying stellar population and become prominent in the spectrum in which A to early-F stars, living up to $\sim$ 1.5 Gyr, contribute significantly. This feature has been exploited to find the signature of poststarbursts in distant galaxies, often using Hδ and/or Hγ absorption due to less contamination from emission filling (e.g., Dressler & Gunn 1983; Zabludoff et al. 1996; Dressler et al. 2004; Goto 2007). The limited spectral baseline makes only low-lying Balmer lines available for our sample. Fig. 14 shows the Na I D velocity as a function of the Hβ spectral line index $W_0(\mathrm{H}\beta)$. A spectral line index is an estimate of the sum of emission and absorption equivalent widths (§ 2.2.1). In the figure, outflows are seen in the following two classes of objects. One class is those with $W_0(\mathrm{H}\beta) < 0$ Å, meaning that Hβ is seen in emission, so they are the outflows seen in star-forming galaxies in the blue cloud (Fig. 10). Another is those with $W_0(\mathrm{H}\beta) \gtrsim 3$ Å, slightly offset from a concentration of objects with systemic Na I D velocity around $W_0(\mathrm{H}\beta) \approx 2$ Å. To put this in perspective, the inset of Fig. 14 shows the evolution of *stellar* Hβ absorption index over a range of stellar ages. A stellar population

with the age $\gtrsim 10$ Gyr has its $W_*(\mathrm{H}\beta)$ asympototing to ≈ 2 Å. The Hβ absorption would be seen at $W_0(\mathrm{H}\beta) \gtrsim 3$ Å during the poststarburst phase from 10 Myr to ~ 2 Gyr. In practice, a measured Hβ index from a galaxy spectrum includes some nebular emission line flux originating from the H II regions surrounding hot, young stars in the presence of residual star formation, pushing a Balmer absorption index to a smaller, less positive value. Therefore, $W_0(\mathrm{H}\beta) \gtrsim 3$ Å objects are likely to be in the poststarburst phase. A large number of systemic Na I D velocity objects around $W_0(\mathrm{H}\beta) \approx 2$ Å is also consistent with old, quiescent galaxies not hosting outflows.

The bottom panel of Fig. 13 shows the relation between the NUV$-R_{\mathrm{AB}}$ color and the Hβ spectral line index for the subset of sample with both measurements. Although the small statistics make interpretation difficult, we can see that the red-sequence objects with outflows appear to have a slightly higher $W_0(\mathrm{H}\beta)$ in general compared to those without. A few blue-sequence objects having NUV$-R_{\mathrm{AB}} < 5.4$, both with and without outflows, also move to the $W_0(\mathrm{H}\beta) > 0$ Å regime. If these objects host residual star formation, inferred from their blue NUV$-R_{\mathrm{AB}}$ color, their emission fluxes may fill Hβ absorption, making the observed $W_0(\mathrm{H}\beta) \approx 2$–3 Å only lower limits to their absorption equivalent strength. This would make the case stronger for the poststarburst identity.

The combination of selection cuts from our sample yields a small number of fully overlapping objects across a variety of measurements and makes it difficult to reach generalizing conclusions with statistical rigor. Nevertheless we do find overwhelming consistency in the evidence that our LIRG-type outflows are mostly seen either in starburst or poststarburst objects. This naturally fits into the currently favored scenario of galaxy evolution between blue-cloud and red-sequence galaxies, in which some mechanism (e.g., merger) triggers a starburst in a blue galaxy which then gets "quenched" by some feedback mechanism, such as by an AGN or supernovae, by the time the galaxy joins the red sequence. The outflows may be the result of such feedback process observed in "transition" objects.

However, we must also note that stronger Balmer absorption only indicates that there was certainly a detectable *enhancement*, relative to the present, of star formation in the recent past; whether or not an individual case makes the criteria for a conventional *starbusrt* is admittedly unclear, especially given our crude diagnostics. There are plausible ways for galaxies to quench star formation without going through a starburst phase, and such mechanisms could generate outflows and detectable enhancement of Balmer absorption, if quenching occurs quickly. This possibility can be explored further only through better diagnostics. [13]

3.4. *Host Morphology*

Fig. 15 shows a subset of galaxies with Na I D measurements for which we have the quantitative morphology from the *HST*/ACS imaging analysis by Lotz et al. (2008). A set of new nonparametric morphology measures, Gini coefficient G which measures the distribution of flux among pixels over a galaxy and the second-order moment of the brightest 20% of the total galaxy flux M_{20}, is calibrated visually to the traditional morphological classifications (Lotz et al. 2004): early-type (E/S0/Sa), late-type (Sb–Ir), and merger candidates. Our survey is more sensitive to luminous, high surface brightness galaxies (§ 2.3), and Fig. 15 shows that the sampling is biased against objects with late-type (i.e., lower surface brightness) morphology; see Lotz et al. (2008) for the analysis of complete samples drawn from the parent AEGIS survey, which shows that the many objects with low surface brightness, late-type morphology, which would appear toward the bottom-left

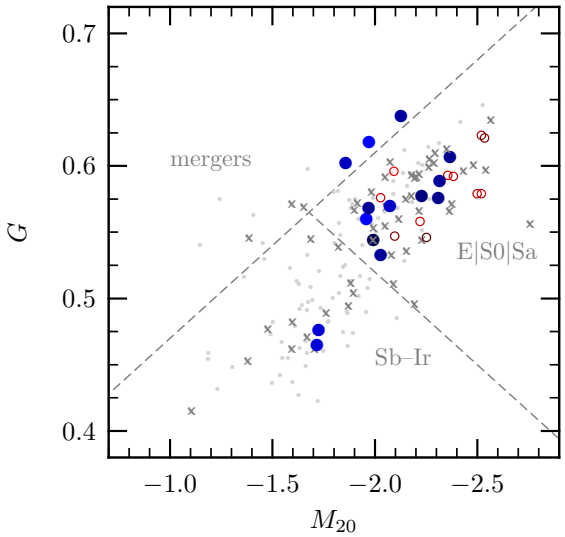

FIG. 15.— Quantitative morphology measure (Gini coefficient G and the second-order moment of the brightest 20% of the total galaxy flux M_{20}) from the analysis of *HST*/ACS images by Lotz et al. (2008). The morphological cuts (*dashed gray lines*) to the "traditional" classes are from Lotz et al. (2008), calibrated with the $z = 0$ rest-frame B-band morphology of their sample. The symbols are as in Fig. 2. (*A color version of this figure is available in the online journal.*)

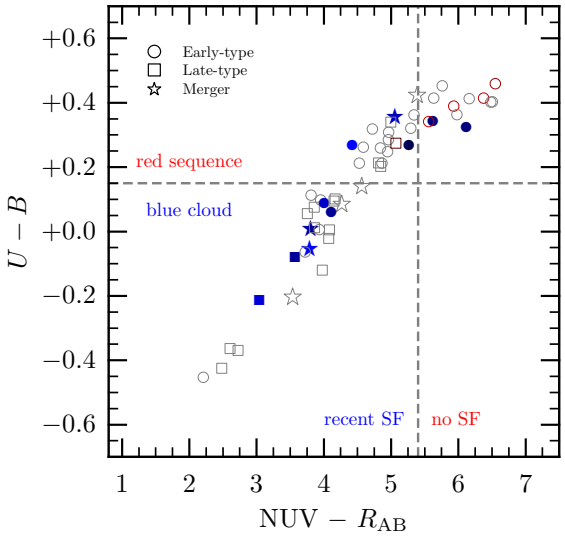

FIG. 16.— Morphology of objects in terms of the rest-frame ($U-B$, NUV$-R_{\mathrm{AB}}$) color-color diagram; see Fig. 13. The morphology, from the analysis of *HST*/ACS images by Lotz et al. (2008), is divided into early-type (E/S0/Sa; *circle*), late-type (Sb–Ir; *square*), and merger-candidates (*star*). The filled symbols indicate host galaxies of outflows. The symbol colors are as in Fig. 2. Only the objects from the high-S/N Na I D velocity sample (§ 2.4.1) with NUV measurements are plotted. (*A color version of this figure is available in the online journal.*)

[13] With our sample, no robust way exists for directly connecting poststarburst to the kind of star formation detected in NUV. The advantage of NUV diagnostics here is its sensitivity to low-level star formation that normally eludes detection in the visible, due to much larger light contribution from old stars to the visible region of galaxy spectrum, and may not tell us much about the timescale over which such low-level star formation has been in existence. Therefore the star formation seen in NUV could be "residual" star formation from a recent starburst/star-forming event or it could just be a small amount of continuous star formation.

corner, did not make our selection cut.

The transition between a LIRG to a ULIRG is physically plausible in the merger sequence (Sanders 2004), so the high outflow detection rate ($3/6 = 0.5 \pm 0.2$) in merger candidates is not surprising. Outflows are detected in almost all local ULIRGs (Martin 2005, 2006; Rupke et al. 2005b). Although all three merger candidates with outflows are detected at 24 μm, only one is a LIRG. Since the dynamical timescale of merger, ~ 1 Gyr, exceeds that of gas consumption, ~ 100 Myr, it is likely that we miss the (U)LIRG phase due to its short duty cycle. It should be noted, however, the nature of the association between mergers/interactions and (U)LIRGs is not as well established for objects at $z \sim 0.5$.

A majority ($9/14 = 0.64 \pm 0.13$) of outflows are seen in the objects with early-type morphology (E/S0/Sa). An insight on the order of morphological transformation may be given by Fig. 16, which plots the distribution of morphology in terms of the rest-frame ($U-B$, NUV$-R_{\rm AB}$) color-color diagram. Consistent with the common knowledge, most late-type galaxies are in the blue cloud, while most early-type galaxies are in the red sequence. The distribution of outflow hosts roughly follows that of the parent sample. Although the small sample size does not allow a statistically robust conclusion, outflows appear to be seen more preferentially where merger candidates are also seen. Previously we find evidence that some outflows are seen in poststarburst objects (§ 3.3). The early-type morphology, coupled with the signs of interaction in a few of the red-sequence outflows, is consistent with the existing studies of poststarburst galaxies as *transition* objects in the morphology sequence, which conclude that they are spheroidal, often showing signs of interaction (e.g., Yang et al. 2004; Goto 2005).

We find only two outflows with late-type morphology, at $z > 0.35$. Fig. 15 makes clear that our selection is highly biased toward high surface brightness galaxies; we have missed a large population of low surface brightness star-forming galaxies that are dim in the rest-frame visible continuum, with which our primary selection cut was made. These outflows with late-type morphology are detected significantly in the infrared, having $\log(L_{\rm IR}/L_\odot) \approx 11.1$ and 10.4. Unlike ULIRGs, the morphology of LIRGs appears to be a mixed bag. At $z \sim 0.7$, however, more than half of their LIRGs have disk morphology (e.g., Bell et al. 2005; Melbourne et al. 2005), suggesting that the abundant LIRG population simply reflects an elevated level of star formation in normal galaxies at an earlier lookback time. All our objects are at lower redshifts, and it is unclear if we are observing disky LIRGs of the type seen at higher redshifts.

4. DISCUSSION

We have seen that the detection rate of LIRG-like outflows is a strong function of infrared luminosity or star formation rate (§ 3.1). The distribution of specific star formation rates at a fixed stellar mass (Fig. 9) might imply that the frequency of outflows may be higher for the objects in which ongoing star-forming activity is enhanced relative to the past average (i.e., high birthrate parameter). The distribution in the optical color magnitude diagram shows that outflows are abundant both in the blue cloud and the red sequence (§ 3.2). The NUV photometry reveals that the red-sequence outflows are hosted by the objects that have gone through recent star formation (Fig. 13). There is evidence that some of the red-sequence outflows are in dusty (Fig. 12), star-forming galaxies (Fig. 11). Yet some may be poststarburst galaxies (§ 3.3) just arriving the red sequence, which is consistent with their early-type morphology (§ 3.4). We now discuss a few fine points that need attention, and describe how our finding of Na I D outflows might fit into the current understanding of galaxy formation and evolution.

4.1. *Redshift Evolution of Outflows*

Fig. 6 shows the detection of outflows as a function of redshift in our sample. Over the redshift range, star-forming properties of galaxies are expected to change and so do the detection rates of outflows. In the figure, no $M_* \approx 10^{11} M_\odot$ galaxies at $z \approx 0.2$ show signs of an outflow, yet a significant fraction of galaxies with the similar mass at $z \approx 0.5$ do. This is consistent with the known trend of the star formation history of galaxies and the increasing trend of outflow detection rate with SFR (§ 3.1). Noeske et al. (2007a) shows that star-forming galaxies with $M_* \approx 10^{11} M_\odot$ are rare at $z < 0.45$ but are abundant and most are LIRGs at $z > 0.45$. Fig. 6 shows that the outflows detected in our sample are typically seen in high-M_* galaxies at higher z with an SFR expected in a LIRG ($\gtrsim 20\ M_*\ {\rm yr}^{-1}$). Due to low S/N, however, we cannot say whether or not lower-M_* galaxies at $z \sim 0.5$ host outflows. Nevertheless, at the high M_* end, we clearly observe that the "downsizing" effect extends to the detection rate of LIRG-like outflows, i.e., the typical mass of galaxies that host outflows move to a lower mass toward lower redshift, much like the trend seen in cosmic star formation history of galaxies (e.g., Madau et al. 1996; Lilly et al. 1996; Le Floc'h et al. 2005; Faber et al. 2007; Noeske et al. 2007a; Cooper et al. 2008). Bundy et al. (2006) qunatify the evolving trend in terms of the "quenching mass limit," which is shown in Fig. 6 for a crude comparison. An important connection is likely to exist between quenching events and gaseous feedback, so the redshift evolution of outflows needs to be explored in view of host galaxy properties.

4.2. *Merger-Triggered Activities and Outflows*

Merger-driven galaxy evolution has been a prominent paradigm over the past decades, and the current success of the ΛCDM theory in describing the hierarchical structure formation certainly points to its significant roles in galaxy-scale phenomena. The relevance of mergers in shaping the cosmic star formation history of galaxies, however, is under intense scrutiny. The difficulty arises from the fact that direct identification of mergers and quantifying their frequency from the observation of high-redshift galaxies remains very challenging, due to a number of factors including surface brightness dimming and shifting passbands. Galaxy mergers of star-forming disk galaxies have attracted much attention, because they are a mechanism widely known to cause enhanced star formation, after which merger remnants dynamically relax into spheroids (e.g., Mihos & Hernquist 1996; Cox et al. 2006). Along with the expected increase of the merger rate with the lookback time from numerical simulations (e.g., Gottlöber et al. 2001), mergers have been invoked as a mechanism responsible for the declining trend of the comoving star formation density since $z \sim 2$ (e.g., Lilly et al. 1996; Madau et al. 1996), although exactly how much mergers contribute to the trend is still debated (e.g., Bridge et al. 2007; Lotz et al. 2008). Galaxy merger is appealing also for it affects star-forming as well as morphological properties of galaxies in ways that naturally explain the observed transition of young (i.e., blue and disky) into old (i.e., red and spheroidal) galaxy populations. In principle, a variety of such

transient phenomena as starburst and quasars can also be integrated into a coherent picture of merger-driven galaxy evolution (e.g., Sanders & Mirabel 1996; Hopkins et al. 2006).

The correlation of the outflow detection rate with the degree of elevation in star-forming activity certainly indicates that starbursts are an important component of galactic superwind phenomenon. However, outflow is exciting not because it is associated with such a spectacular starburst event, but because it may carry away from the host galaxy the bulk of "fuel" for further star formation, which may contribute to the "quenching" of star formation. In fact, ULIRGs (i.e., gas-rich mergers) show dynamical evidence for spheroids in formation (e.g., Genzel et al. 2001), and the star formation history of poststarburst galaxy is consistent with the (U)LIRG origin (e.g., Poggianti & Wu 2000; Bekki et al. 2001; Kaviraj et al. 2007). Our detection of Na I D outflows in poststarburst galaxies strongly suggests that feedback mechanism affects the kinematics of cool interstellar gas well after the most intense phase of star formation. The fact that quite a few red-sequence galaxies host winds may not be surprising yet still a striking result. A vast majority of absorption-line studies of outflows in literature has been on vigorously star-forming systems. Using a plot similar to Fig. 1, Rupke et al. (2005a) showed that most outflows in infrared-selected galaxies were detected in the loci of low Mg I b and high Na I D absorption indices, i.e., young galaxies with high interstellar Na I D column (their Fig. 8). In contrast, the red-sequence galaxies with outflows in our sample can have a high Mg I b absorption index, reflecting the presence of intermediate to old stellar population, and are not clearly distinct from other red-sequence galaxies in an optical color magnitude diagram (Fig. 10). The apparent connection between outflows and high M_* poststarburst galaxies provides circumstantial evidence that outflows of cool gas contributes to or is a consequence of more effective quenching of star formation.

How the progenitors of spheroidal galaxies in the local universe evolve into their current state remains a topic under vigorous investigation. While their stellar contents suggest that massive spheroids have been passively evolving and that their stellar mass changes little since $z \sim 1$ (e.g., Brinchmann & Ellis 2000; Bundy et al. 2005), the evolution of the luminosity function suggests that the number density of luminous red galaxies has increased by a factor of ~ 2 over the same period (e.g., Bell et al. 2004; Brown et al. 2007; Faber et al. 2007). Over the similar redshift range, star-forming galaxies have a relatively small spread in SFRs at a fixed mass in the blue sequence (e.g., Noeske et al. 2007a), leading to a paucity of objects presumably in transition between the blue and red sequences. Furthermore, less massive spheroids have younger stellar contents (e.g., Treu et al. 2005; Kaviraj et al. 2008) and the characteristic galaxy mass above which the star formation in galaxies quenched evolves over redshift in a downsizing fashion (Bundy et al. 2006), indicating that catastrophic transition events occur at a progressively lower mass toward lower redshift. The exact rate of transition is very difficult to estimate, yet indirect arguments favor rare and/or fast mechanism(s) (e.g., Blanton 2006). Gas-rich mergers perhaps contribute to some but not all of these blue-red transitions (Bundy et al. 2007). The qualitatively similar downsizing trend in star-forming galaxies and outflow hosts over $z < 0.5$ (§ 4.1), however, may imply that the mechanism responsible for downsizing of star formation may also accompany outflows. A rigorous conclusion must await the quantitative analysis of the sample which suffers less from small number statistics, selection effects, and incompleteness.

We must also note that it is not clear that merger per se is a necessary precursor for outflows. The direct morphological evidence for interaction is not very strong in our outflows (a majority of outflows are in early-type galaxies; § 3.4). A circumstantial evidence is provided only through an indirect argument that a spheroidal formation follows a merger-induced starburst with a poststarburst signature. Since the timescale for mergers at high redshift to remain identifiable is shorter than a poststarburst phase, the scarcity of direct evidence may not immediately discount the importance of mergers. However, it is possible that low-level star formation in early-type galaxies could drive outflows, perhaps via the accretion of gas-rich satellites or minor mergers. Early-type galaxies also have reservoirs of hot gas, which could provide fuel for star formation via condensation. It has been suggested that the early-type galaxy population itself shows bimodality in their UV-visible color distribution, reflecting the richness in their star formation histories; low-level star formation appears to continue in less-massive early-type galaxies (Kaviraj et al. 2008). The origin of outflows in the red galaxies may not be as simple as a quenching event followed by passive evolution.

Furthermore, the mounting evidence now shows that a majority of $z \sim 1$ LIRGs are normal disk galaxies whose elevated star formation is *not* caused by interaction (e.g., Bell et al. 2005; Lotz et al. 2008). The gradual decline of star-forming efficiency in their disks may be responsible for much of the global trend seen in comoving SFR density. From our study alone, whether or not these disky LIRGs at high-redshift host outflows is not clear; the nature of outflows in these objects may be different from merger-induced ones.

It would be interesting to see how the presence of outflows at $z \lesssim 1$ contribute to the fate of $z \sim 1$ LIRGs down to $z \sim 0$, which may either stay but fade gradually within the blue sequence or go through rapid quenching of star formation to migrate to the red sequence. Given the strong evolution of galaxy properties in general (§ 4.1), our knowledge from the local study of LIRG-like outflows might not be relevant for high-z, disky LIRGs. On the other hand, if the outflow strength correlates with some parameter such as the presence of nuclear activity or their degree of interaction in relation to their morphology among high-z LIRGs [as observed in local ULIRGs by Martin (2005)], deprivation of (cool) gas via superwind may be important in transforming star-forming disks into quiescent spheroids in catastrophic events at those redshifts. The detection rate of outflows in view of host galaxy morphology at $z \lesssim 1$ may provide some insight on the physical mechanism that maintains the bimodality in galaxy population since $z \sim 1$. A comparison of mass outflow rates in $z \sim 1$ LIRGs with different morphology would also make an interesting exercise to put some constraint on the role of mass loading in the evolutionary histories of morphology and star formation. Fortunately, several useful UV resonance lines at different ionization states shift into visible window for $z \sim 1$ objects (e.g., Weiner et al. 2009), so future surveys are in a better position to constrain mass loading from these lines (e.g., Murray et al. 2007).

4.3. *Star Formation Versus AGN*

It is usually assumed that superwinds are driven by thermalized energy output from supernovae. In principle, AGNs offer much larger repository of energy than supernovae, and the ubiquity of supermassive black holes in galactic spheroids inferred from the $M_{\rm bh}$-σ_v relation (e.g., Tremaine et al. 2002)

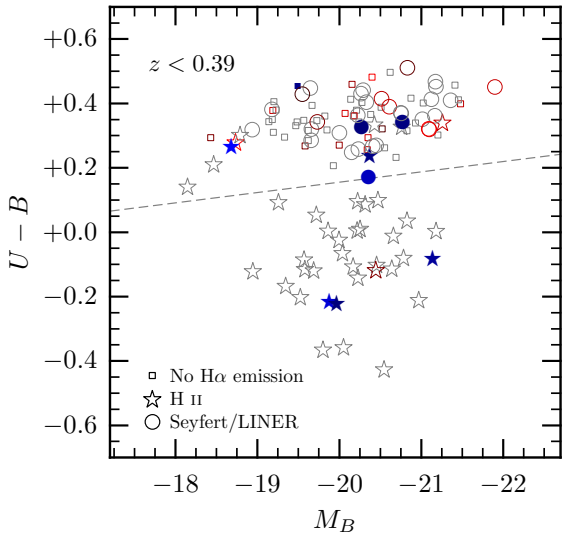

FIG. 17.— Rest-frame ($U-B, M_B$) color-magnitude diagram for the objects in the high-S/N sample with [N II]/Hα emission equivalent width ratio; see § 4.3. The spectral baseline restricts the [N II]/Hα measurements to $z < 0.39$ objects. The symbols indicate the equivalent width ratio of Seyfert/LINER [log([N II]/Hα) ≥ –0.3; *circle*] and H II-region [log([N II]/Hα) < –0.3; *star*]; the objects without detectable Hα emission do not have equivalent width ratios (*square*). The colors are as in Fig. 2, and outflows are marked by filled symbols. (*A color version of this figure is available in the online journal.*)

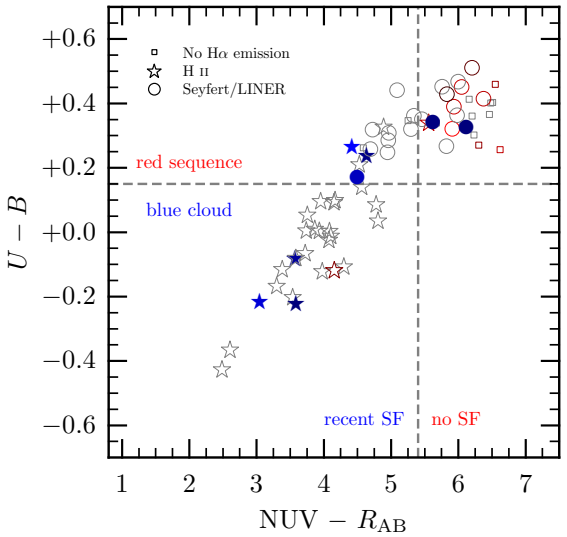

FIG. 18.— Rest-frame ($U-B$, NUV$-R_{AB}$) color-color diagram for the objects in the high-S/N sample with [N II]/Hα emission equivalent width ratio. Symbol shapes are as in Fig. 17. Symbol colors are as in Fig. 2, and outflows are marked by the filled symbols. The photometric color delineations are described in the caption of Fig. 13. The spectral baseline restricts the [N II]/Hα measurements to $z < 0.39$ objects. (*A color version of this figure is available in the online journal.*)

and their co-evolution with the lookback time (e.g., Woo et al. 2006) suggests that the energy output from AGNs may play important roles in galaxy formation. While AGNs offer increasingly attractive solutions to the yet elusive mechanism for shutting off star formation in massive objects, where and how their energy output couples to the gas in and around galaxies remains to be identified. Recently, however, several observational studies have elucidated the connection between poststarburst and nuclear activity: host galaxies of quasars often show poststarburst signature in their continuum emission (e.g., Canalizo et al. 2006); the morphology of poststarburst galaxies often show a blue core, which produces a LINER spectrum (Yang et al. 2006); the optical emission-line ratios classify a majority of poststarburst galaxies into Seyfert/LINERs (Tremonti et al. 2005; Yan et al. 2006; Yan & DEEP2 Team 2006).

Low-ionization outflows are found to be faster in starburst galaxies with some indication of AGN (Martin 2005; Rupke et al. 2005b). In $z \sim 0.5$ poststarburst galaxy sample, Tremonti et al. (2007) find Mg II outflows of ~ 1000 km s^{-1}, much faster than the typical Na I D outflows in ULIRGs ($\sim$ 300–400 km s^{-1}). These fast outflows in the galaxies at their *postquasar* phase provide compelling evidence for AGN-driven outflows in poststarbursts. It is worth noting that, due to the difference in sample selection, our poststarburst outflows in general are likely to be of a more typical kind than those of Tremonti et al., i.e., the event which led to the suppression of star formation does not have to accompany quasar activity for us to classify them as poststarbursts. Although the exact values are physically meaningless (§ 2.5), our measurements imply Na I D outflow velocities of ~ 100 km s^{-1}, which do not favor one scenario over others as to the outflow driving mechanism. It is plausible that some of our red-sequence outflows have gone through the kind of postquasar phase that Tremonti et al. observed, but they do not all have to be.

Nonetheless, the fact that typical poststarburst galaxies show low-level nuclear activity seems convincing, given the recent studies of the line emission from red-sequence galaxies. In Fig. 17, we show the classification of Seyfert/LINER versus star formation using the [N II]/Hα emission *equivalent width* ratio, such that log([N II]/Hα) = –0.3 divides the two classes.[14] The spectral baseline restricts the [N II]/Hα measurements to $z < 0.39$ objects. The use of [O III]/Hβ allows us to extend the classification to $z > 0.39$ objects in which we see a majority of outflows, but the delineation of Seyfert/LINER and star formation becomes notoriously ambiguous when only that ratio is used. A comparison to Weiner et al. (2007) shows that *all* $z > 0.35$ outflows in our sample have H II-region–like ratios in [O III]/Hβ, which is rather puzzling, given many of them are red galaxies where line emissions tend to originate from AGN/LINERs, according to local studies. Using [N II]/Hα, Fig. 17 shows a distribution of objects grossly consistent with Yan et al. (2006); i.e., line emission from the red sequence is dominated by Seyfert/LINER, while that from the blue cloud is mostly from star formation. Host galaxies of outflows appear to follow the parent distribution, yet the analysis suffers from small number statistics.

In Fig. 18, we have a slightly different view on the color distribution of galaxies in terms of the emission excitation. The advantage of adding the near-UV photometry to detect low-level star formation has been discussed in § 3.2. The small number of outflow host galaxies at $z < 0.39$ still limits our interpretation. Nevertheless, it is quite interesting that the transition from star formation to Seyfert/LINER, and then to no Hα emission appears to happen along the stellar age sequence, and the abundance of Seyferts/LINERs is observed in the region occupied by the galaxies in transition, a significant fraction of which appears to host outflows at $z \sim 0.5$ (Fig. 13). Although the temporal co-existence of relic outflows and cur-

[14] Unfluxed DEEP2 spectra force us to use equivalent widths in place of line fluxes, yet the adjacent lines forming the ratios are so close that they give similar results (Kobulnicky & Phillips 2003). The Hα-[N II] complex is fitted with three Gaussians for emission lines. When Hα absorption is obviously present, another Gaussian is fitted; otherwise, a fiducial rest-frame equivalent width of 2 ± 1 Å is added to the Hα emission flux.

rent nuclear activity does not necessarily imply any causal connection, extending this analysis to higher redshift, where more outflows are expected, could help us understand the potential impact of winds in establishing the observed trend in terms of their driving mechanisms.

The presence of inflows in red, early-type (Fig. 15) galaxies in the above figures is also remarkably consistent with their host either being quiescent or having their optical emission lines excited by AGN/LINERs, with little evidence for star formation. It remains to be seen whether any evidence exists to directly connect the inflows and the nuclear activities. On the other side of outflows, the nature of inflows also needs to be explored, since it has been long speculated that some mechanism, an AGN being a prime suspect, is preventing more stars from being formed than observed in massive elliptical galaxies.

5. SUMMARY

We reported on a S/N-limited search for low-ionization outflows using the DEEP2 spectra of the $0.11 < z < 0.54$ objects in the AEGIS survey. Doppler shifts from the host galaxy redshifts were systematically searched for in the Na I D optical resonance absorption doublet. This was the very first time that a signature of galactic superwind was systematically looked for in the individual galaxy spectra from a modern, large spectroscopic redshift survey.

Our Na I D profile fitting method closely followed that of Rupke et al. (2005a), explicitly fitting the absorption line model parameterized by the wavelength and the optical depth at the line center, Doppler width, and covering fraction in a self-consistent manner. The confidence intervals in the Na I D velocities were estimated through the MCMC sampling technique. This allowed us to evaluate the quality of Na I D velocity measurements visually in terms of probability distributions of model parameters. Although the spectral resolution and S/N limited us to studying the interstellar gas kinematics by fitting a single doublet component to each observed Na I D profile, LIRG-like outflows should have been detected at $\gtrsim 6\sigma$ in absorption equivalent width down to the survey limiting S/N (~ 5 pixel^{-1}) in the continuum around Na I D. This meant that, if a Na I D outflow of a comparable strength to the LIRGs detected by the Rupke et al. (2005b) survey left its signature in a spectrum, we were able to detect the presence in our survey. We discussed the challenges involved in recovering physically important parameters from a moderate S/N spectrum yet argued that a Doppler shift could be measured robustly.

The detection rate of LIRG-like outflow clearly showed an increasing trend with star-forming activity and infrared luminosity. However, by virtue of not selecting our sample on star formation, we also found a significant fraction of outflows in galaxies on the red sequence in the rest-frame ($U-B$, M_B) color-magnitude diagram. Most of these red-sequence outflows were of early-type morphology and showed the sign of recent star formation in their UV-optical colors; some showed enhanced Balmer Hβ absorption lines indicative of poststarburst as well as high dust extinction.

We also note that inflows were detected in some red, early-type galaxies. Although the definition of an inflow in this study was just symmetrically opposite to that of an outflow, the fact that we observed them in very distinct subsets of galaxies strongly indicated that our outflow/inflow detections were not spurious. However, with the difficulty in removing stellar absorption component at Na I D as well as the lack of immediate explanations for their driving mechanisms, the investigation of inflows was beyond the scope of this paper and will be explored in future AEGIS studies. We merely note that a connection is suspected between an inflow and the feeding of nuclear activity in the maintenance mode of AGN feedback.

The fact that many of our outflows have been found in galaxies presumably in transition suggests that galactic superwinds could outlive starbursts and play a role in quenching star formation in the host galaxies on their way to the red sequence. The detectable imprints of gaseous feedback in these galaxies provide us a means to observationally constrain different feedback models. Despite that the small number statistics as well as selection effects hindered our ability to rigorously characterize the nature of the host galaxies of outflows across a wide array of physical parameters accessible in the AEGIS survey, the initial analysis presented in this paper will help design future experiments on the impact of superwinds on galaxy evolution in the epoch when the star-forming properties of galaxies drastically change since $z \sim 1$. Gaseous kinematics adds to future studies a useful dimension to explore and opens up a promising avenue for constraining the driving mechanisms of baryons cycling through the components that constitute the luminous part of the universe, as well as for directly quantifying how much gas joins in such process.

T.S. would like to thank the following scientists for inspirations: Christy Tremonti for sharing her stimulating results on SDSS Na I D outflows, as well as her hospitality during his visits to Steward; Philip Marshall for enlightenment with the Bayesian statistical methods; and David Rupke and his coworkers for the series of detailed work on Na I D outflows. T.S. gratefully acknowledges Alison Coil for her thorough reading of the manuscript and her very insightful suggestions and also wishes to extend his thanks to Ben Weiner, Sandy Faber, and François Schweizer for helpful discussions. We thank the anonymous referee for his or her thorough reading, constructive feedback, as well as patience. This work was never possible without the dedicated efforts, contributions, as well as the generosity from all the AEGIS/DEEP2 members.

The research presented in this paper made an extensive use of the Python programming language and the associated tools. PyRAF and PyFITS are products of the Space Telescope Science Institute, which is operated by AURA for NASA. The figures in this paper are all prepared by PyTioga[15], an open source software for creating figures and plots using Python, PDF, and TeX.

This research has made use of the NASA Astrophysics Data System abstract service.

Financial support was provided by the David and Lucille Packard Foundation.

Funding for the DEEP2 survey has been provided by NSF grant AST-0071048 and AST-0071198. Some of the data presented herein were obtained at the W.M. Keck Observatory, which is operated as a scientific partnership among the California Institute of Technology, the University of California and the National Aeronautics and Space Administration. The Observatory was made possible by the generous financial support of the W.M. Keck Foundation.

We gratefully acknowledge NASA's support for construction, operation, and science analysis of the *GALEX* mission,

[15] PyTioga is available at http://pytioga.sourceforge.net/.

developed in cooperation with the Centre National d'Etudes Spatiales of France and the Korean Ministry of Science and Technology.

For the full acknowledgement of the AEGIS data set, please refer to Davis et al. (2007).

Last but not least, we recognize and acknowledge the very significant cultural role and reverence that the summit of Mauna Kea has always had within the indigenous Hawaiian community. We are most fortunate to have the opportunity to conduct observations from this mountain.

APPENDIX

MODELING THE Na I D ABSORPTION LINE

We closely follow the model presented by Rupke et al. (2002, 2005a); readers are strongly encouraged to refer to these papers for a thorough discussion. Only a single component of the Na I D doublet is fitted in each spectrum; that is, we assume that our fitting of one absorption doublet is sensitive to the bulk property of the multiple Na I D absorbing clouds integrated along the sightline. While this is certainly an oversimplification (see, e.g., Rupke et al. 2002, for how complex an absorption profile with several kinematic components can appear), the limited S/N does not allow more detailed analysis; for the cases in which observed Na I D absorption lines are well defined, the fitting results are reliable. For the sole purpose of detecting a Doppler shift from a systemic redshift (and *not* measuring the exact velocity value), a single component fit is an acceptable compromise. We are effectively addressing whether an observed Na I D line profile can accommodate a single Doppler-shifted Na I D absorber.

The observed intensity profile $I(\lambda)$ of an absorption line is fitted by a model profile parameterized in the optical depth space. That is, if the (velocity-independent) partial covering fraction is C_f, each Na I D doublet is modeled by

$$I(\lambda) = 1 - C_f \left[1 - e^{-\tau_{\rm blue}(\lambda) - \tau_{\rm red}(\lambda)}\right] ,$$

where $\tau_{\rm blue}(\lambda)$ and $\tau_{\rm red}(\lambda)$ are the optical depths of blue and red components of the doublet as a function of wavelength λ. (This expression is appropriate for a continuum-divided spectrum.) We assume that the velocity distribution of absorbing atoms within a cloud is Maxwellian, such that each absorption line is modeled as

$$\tau(\lambda) = \tau_0 e^{-(\lambda-\lambda_0)^2/(\lambda_0 b_D/c)^2} ,$$

where τ_0 is the optical depth at the line center λ_0, c the speed of light, and b_D is the Doppler parameter in units of speed. Since the ratio of oscillator strengths for blue and red sides of the Na I D doublet is two (Morton 1991), we may assume that the central optical depths are related via $\tau_{0,\rm blue}/2 = \tau_{0,\rm red}$. Hence the intensity profile of each Na I D doublet component is

$$I(\lambda) = 1 - C_f \left\{1 - \exp\left[-2\tau_0 e^{-(\lambda-\lambda_{\rm blue})^2/(\lambda_{\rm blue} b_D/c)^2} - \tau_0 e^{-(\lambda-\lambda_{\rm red})^2/(\lambda_{\rm red} b_D/c)^2}\right]\right\} ,$$

where $\lambda_{\rm blue}$ = 5889.9512 Å and $\lambda_{\rm red}$ = 5895.9243 Å are the rest-frame central wavelengths (in air) of blue and red lines of Na I D doublet. As noted by Rupke et al. (2005a), the Maxwellian velocity distribution and velocity-independence of partial covering fraction are significant assumptions. In case there is an outflow, an observed Na I D absorption profile likely arises from several absorbing clouds entrained in a superwind (e.g., A. Fujita et al. 2008, in preparation), so their bulk kinematics would not be described simply by a Maxwellian distribution. Furthermore, if for example a spherical virialized cloud cuts through a sightline, the covering fraction must depend on the velocity of the constituent particles in the cloud; thus the assumption of velocity independence for covering fraction is not physically consistent in detail. Nevertheless, our analysis does not benefit from relaxing these constraints, as the quality of data does not warrant that such detailed information can be extracted.

Before the above model is fitted, each spectrum around Na I D is divided by the pseudocontinuum, a straight line fitted to the variance-weighted spectra within the rest-frame regions of 5822–5842 Å and 5910–5930 Å; the ranges are chosen after visual inspection for the best continuum normalization centered around Na I D, while avoiding other prominent stellar absorption features as much as possible. In a very strong outflow, the nebular emission line He I λ 5876 can contaminate the bluest wing of a Doppler-shifted Na I D component. Visual inspection indicates that few spectra suffer from such a contamination, so no account is taken for the He I emission in our measurements.

We take $\lambda_{\rm red}$, b_D, τ_0, and C_f as model parameters to be estimated via the Metropolis-Hastings algorithm (Metropolis et al. 1953; Hastings 1970), which yields a more robust confidence interval on a model parameter than that derived from a covariance matrix, when the probability distribution of the model parameter cannot be described as Gaussian. The sampling method also improves over Rupke et al. in a sense that each Monte Carlo realization is not drawn from the "best" model which needs to be chosen a priori via least-square fitting, for example. The priors for the model parameters are assumed to have a uniform probability density over their upper and lower limits: 42 km s^{-1} $< b_D <$ 700 km s^{-1}, $0 < \tau_0 < 10^3$, $0 < C_f < 1$, and λ_0 is constrained to be within $\pm$700 km s^{-1} of the systemic velocity. The χ^2 probability distribution for the given degrees of freedom (i.e., the number of data points fitted minus the number of model parameters) is assumed for the likelihood function. Each sampling consists of 10^5 iterations.

The measurement pipeline is built on top of PyMC,[16] which implements the Metropolis-Hasting algorithm as an MCMC sampler, and developed in Python. The distributions of model parameters are visually inspected with a graphical user interface (GUI) along various dimensions; see Fig. 19. The integrity of fitting to the data spectrum is checked at several interactively picked points on the two-dimensional intensity map of the distributions of model parameters. The GUI-driven visual inspection guards against the fits latching on to low-S/N features and helps to identify unphysical fit results. The distribution of $\lambda_{\rm red}$, marginalized over all the other parameters and convolved with the redshift uncertainty, needs to be roughly Gaussian and well bounded within $\pm$700 km s^{-1} to make it into the high-S/N Na I D velocity sample (§ 2.4). The software may be open sourced at a later date.

REFERENCES

Adelman-McCarthy, J. K., et al. 2006, ApJS, 162, 38

Armus, L., Heckman, T. M., & Miley, G. K. 1989, ApJ, 347, 727

[16] The code and documentation are available at http://trichech.us/.

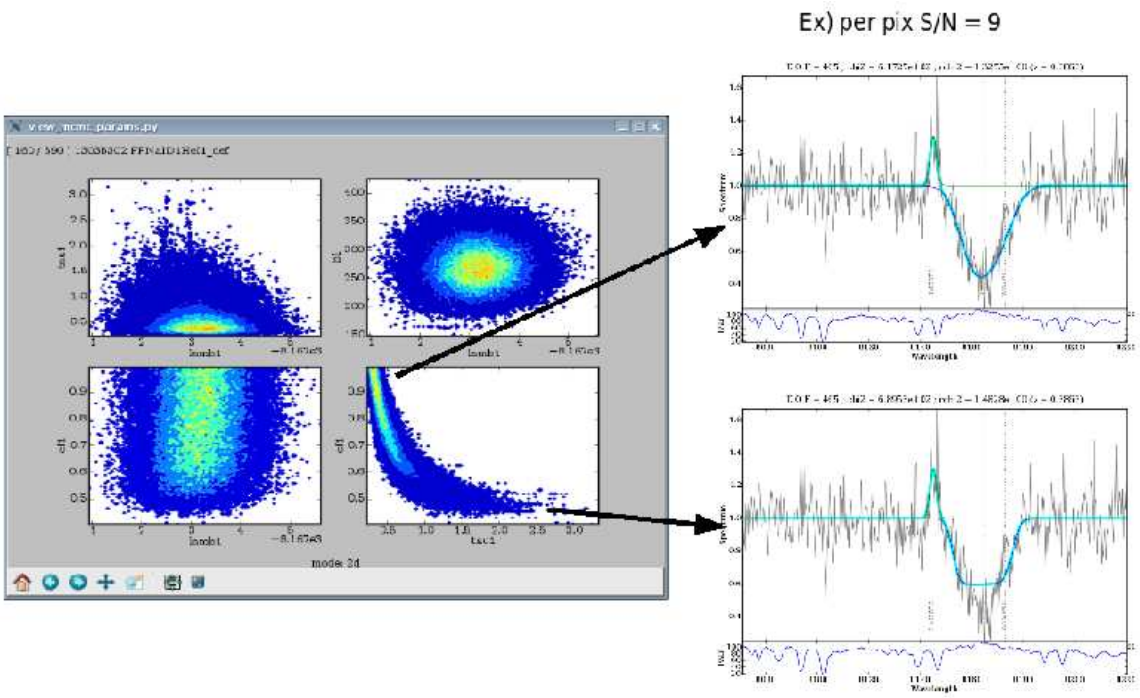

FIG. 19.— Few output windows from the Na I D measurement pipeline. In this figure, the distributions of model parameters are shown as the two-dimensional intensity color maps. Any location on the graphical user interface (*left*) can be clicked on to extract the model spectrum overlayed on top of the data spectrum (*right*). The relatively high-$(S/N)_{pix}$ spectrum yields well-behaving parameter distributions here. The figure also gives an example of typical model parameter distributions. On the left, the parameters plotted are τ_0-λ_{red} (*top left*), b_D-λ_{red} (*top right*), C_f-λ_{red} (*bottom left*), and C_f-τ_0 (*bottom right*). If marginalized over the parameter against which they are plotted, the distributions of λ_{red} and b_D become roughly Gaussian, where as those of C_f and τ_0 are not. It is apparent that C_f is not well constrained for $C_f \gtrsim 0.45$, and τ_0, while relatively well constrained, is highly correlated with C_f. See § 2.4 for detail. (*A color version of this figure is available in the online journal.*)

Baldry, I. K., Glazebrook, K., Brinkmann, J., Ivezić, Ž., Lupton, R. H., Nichol, R. C., & Szalay, A. S. 2004, ApJ, 600, 681
Balogh, M. L., Baldry, I. K., Nichol, R., Miller, C., Bower, R., & Glazebrook, K. 2004, ApJ, 615, L101
Balogh, M. L., Miller, C., Nichol, R., Zabludoff, A., & Goto, T. 2005, MNRAS, 360, 587
Bekki, K., Shioya, Y., & Couch, W. J. 2001, ApJ, 547, L17
Bell, E. F., et al. 2004, ApJ, 608, 752
Bell, E. F., et al. 2005, ApJ, 625, 23
Blanton, M. R. 2006, ApJ, 648, 268
Bower, R. G., Benson, A. J., Malbon, R., Helly, J. C., Frenk, C. S., Baugh, C. M., Cole, S., & Lacey, C. G. 2006, MNRAS, 370, 645
Bridge, C. R., et al. 2007, ApJ, 659, 931
Brinchmann, J., Charlot, S., White, S. D. M., Tremonti, C., Kauffmann, G., Heckman, T., & Brinkmann, J. 2004, MNRAS, 351, 1151
Brinchmann, J., & Ellis, R. S. 2000, ApJ, 536, L77
Brown, M. J. I., Dey, A., Jannuzi, B. T., Brand, K., Benson, A. J., Brodwin, M., Croton, D. J., & Eisenhardt, P. R. 2007, ApJ, 654, 858
Bruzual, G., & Charlot, S. 2003, MNRAS, 344, 1000
Bundy, K., Ellis, R. S., & Conselice, C. J. 2005, ApJ, 625, 621
Bundy, K., Treu, T., & Ellis, R. S. 2007, ApJ, 665, L5
Bundy, K., et al. 2006, ApJ, 651, 120
Canalizo, G., Stockton, A., Brotherton, M. S., & Lacy, M. 2006, New Astronomy Review, 50, 650
Chary, R., & Elbaz, D. 2001, ApJ, 556, 562
Chevalier, R. A., & Clegg, A. W. 1985, Nature, 317, 44
Coil, A. L., et al. 2004, ApJ, 609, 525
Coil, A. L., et al. 2008, ApJ, 672, 153
Cooper, M. C., et al. 2007, MNRAS, 376, 1445
Cooper, M. C., et al. 2008, MNRAS, 383, 1058
Cowie, L. L., Songaila, A., Hu, E. M., & Cohen, J. G. 1996, AJ, 112, 839
Cox, T. J., Jonsson, P., Primack, J. R., & Somerville, R. S. 2006, MNRAS, 373, 1013
Croton, D. J., et al. 2006, MNRAS, 365, 11
Cuillandre, J.-C., Luppino, G., Starr, B., & Isani, S. 2001, SF2A-2001: Semaine de l'Astrophysique Francaise, 605
Davis, M., Gerke, B. F., & Newman, J. A. 2004, ArXiv Astrophysics e-prints, arXiv:astro-ph/0408344
Davis, M., et al. 2003, Proc. SPIE, 4834, 161
Davis, M., et al. 2007, ApJ, 660, L1
Delgado, R. M. G., Cerviño, M., Martins, L. P., Leitherer, C., & Hauschildt, P. H. 2005, MNRAS, 357, 945
Dressler, A., & Gunn, J. E. 1983, ApJ, 270, 7
Dressler, A., Oemler, A. J., Poggianti, B. M., Smail, I., Trager, S., Shectman, S. A., Couch, W. J., & Ellis, R. S. 2004, ApJ, 617, 867
Faber, S. M., et al. 2003, Proc. SPIE, 4841, 1657
Faber, S. M., et al. 2007, ApJ, 665, 265
Genzel, R., Tacconi, L. J., Rigopoulou, D., Lutz, D., & Tecza, M. 2001, ApJ, 563, 527
Goto, T. 2005, MNRAS, 357, 937
Goto, T. 2007, MNRAS, 381, 187
Gottlöber, S., Klypin, A., & Kravtsov, A. V. 2001, ApJ, 546, 223
Hastings, W. K. 1970, Biometrika, 57, 97
Heckman, T. M., Armus, L., & Miley, G. K. 1990, ApJS, 74, 833
Heckman, T. M., Lehnert, M. D., Strickland, D. K., & Armus, L. 2000, ApJS, 129, 493
Heckman, T. M., Sembach, K. R., Meurer, G. R., Strickland, D. K., Martin, C. L., Calzetti, D., & Leitherer, C. 2001, ApJ, 554, 1021
Hopkins, P. F., Hernquist, L., Cox, T. J., Di Matteo, T., Robertson, B., & Springel, V. 2006, ApJS, 163, 1
Horne, K. 1986, PASP, 98, 609
Kaviraj, S., Kirkby, L. A., Silk, J., & Sarzi, M. 2007, MNRAS, 382, 960
Kaviraj, S., et al. 2008, MNRAS, 388, 67
Kennicutt, R. C., Jr. 1998, ARA&A, 36, 189
Kobulnicky, H. A., & Phillips, A. C. 2003, ApJ, 599, 1031
Kurtz, M. J., & Mink, D. J. 1998, PASP, 110, 934
Le Floc'h, E., et al. 2005, ApJ, 632, 169
Lilly, S. J., Le Fevre, O., Hammer, F., & Crampton, D. 1996, ApJ, 460, L1
Lotz, J. M., Primack, J., & Madau, P. 2004, AJ, 128, 163
Lotz, J. M., et al. 2008, ApJ, 672, 177
Madau, P., Ferguson, H. C., Dickinson, M. E., Giavalisco, M., Steidel, C. C., & Fruchter, A. 1996, MNRAS, 283, 1388
Martin, C. L. 2005, ApJ, 621, 227
Martin, C. L. 2006, ApJ, 647, 222
Melbourne, J., Koo, D. C., & Le Floc'h, E. 2005, ApJ, 632, L65
Metropolis, N., et al. 1953, J. Chem. Phys., 21, 1087
Mihos, J. C., & Hernquist, L. 1996, ApJ, 464, 641
Morton, D. C. 1991, ApJS, 77, 119
Murray, N., Martin, C. L., Quataert, E., & Thompson, T. A. 2007, ApJ, 660, 211

Noeske, K. G., et al. 2007, ApJ, 660, L43
Noeske, K. G., et al. 2007, ApJ, 660, L47
Poggianti, B. M., Bressan, A., & Franceschini, A. 2001, ApJ, 550, 195
Poggianti, B. M., & Wu, H. 2000, ApJ, 529, 157
Rieke, G. H., et al. 2004, ApJS, 154, 25
Rupke, D. S., Veilleux, S., & Sanders, D. B. 2002, ApJ, 570, 588
Rupke, D. S., Veilleux, S., & Sanders, D. B. 2005, ApJS, 160, 87
Rupke, D. S., Veilleux, S., & Sanders, D. B. 2005, ApJS, 160, 115
Sanders, D. B. 2004, Advances in Space Research, 34, 535
Sanders, D. B., & Mirabel, I. F. 1996, ARA&A, 34, 749
Sato, T., & Martin, C. L. 2006, ApJ, 647, 946
Schawinski, K., et al. 2006, ArXiv Astrophysics e-prints, arXiv:astro-ph/0601036
Schwartz, C. M., & Martin, C. L. 2004, ApJ, 610, 201
Schwartz, C. M., Martin, C. L., Chandar, R., Leitherer, C., Heckman, T. M., & Oey, M. S. 2006, ApJ, 646, 858
Seibert, M., et al. 2005, ApJ, 619, L55
Shapley, A. E., Steidel, C. C., Pettini, M., & Adelberger, K. L. 2003, ApJ, 588, 65
Tonry, J., & Davis, M. 1979, AJ, 84, 1511
Tremaine, S., et al. 2002, ApJ, 574, 740
Tremonti, C., Kennicutt, R., & Heckman, T. 2005, Starbursts: From 30 Doradus to Lyman Break Galaxies, 329, 80P
Tremonti, C. A., Moustakas, J., & Diamond-Stanic, A. M. 2007, ApJ, 663, L77
Tremonti, C. A., et al. 2004, ApJ, 613, 898
Treu, T., et al. 2005, ApJ, 633, 174
van Gorkom, J. H., Knapp, G. R., Ekers, R. D., Ekers, D. D., Laing, R. A., & Polk, K. S. 1989, AJ, 97, 708
Veilleux, S., Cecil, G., & Bland-Hawthorn, J. 2005, ARA&A, 43, 769
Veilleux, S., Kim, D.-C., Sanders, D. B., Mazzarella, J. M., & Soifer, B. T. 1995, ApJS, 98, 171
Weiner, B. J., et al. 2005, ApJ, 620, 595
Weiner, B. J., et al. 2007, ApJ, 660, L39
Weiner, B. J., et al. 2009, ApJ, 692, 187
Willmer, C. N. A., et al. 2006, ApJ, 647, 853
Woo, J.-H., Treu, T., Malkan, M. A., & Blandford, R. D. 2006, ApJ, 645, 900
Yan, R., & DEEP2 Team 2006, Bulletin of the American Astronomical Society, 38, 1159
Yan, R., Newman, J. A., Faber, S. M., Konidaris, N., Koo, D., & Davis, M. 2006, ApJ, 648, 281
Yang, Y., Tremonti, C. A., Zabludoff, A. I., & Zaritsky, D. 2006, ApJ, 646, L33
Yang, Y., Zabludoff, A. I., Zaritsky, D., Lauer, T. R., & Mihos, J. C. 2004, ApJ, 607, 258
Zabludoff, A. I., Zaritsky, D., Lin, H., Tucker, D., Hashimoto, Y., Shectman, S. A., Oemler, A., & Kirshner, R. P. 1996, ApJ, 466, 104